Reaction Chemistry & Engineering

Linking fundamental chemistry and engineering to create scalable, efficient processes

Accepted Manuscript

Published on 09 November 2026

Licensed under CC-BY 4.0

Check for updates



This is an Accepted Manuscript, which has been through the Royal Society of Chemistry peer review process and has been accepted for publication.

Accepted Manuscripts are published online shortly after acceptance, before technical editing, formatting and proof reading. Using this free service, authors can make their results available to the community, in citable form, before we publish the edited article. We will replace this Accepted Manuscript with the edited and formatted Advance Article as soon as it is available.

You can find more information about Accepted Manuscripts in the Information for Authors.

Please note that technical editing may introduce minor changes to the text and/or graphics, which may alter content. The journal's standard Terms & Conditions and the Ethical guidelines still apply. In no event shall the Royal Society of Chemistry be held responsible for any errors or omissions in this Accepted Manuscript or any consequences arising from the use of any information it contains.

Direct vs. indirect dimethyl ether synthesis from sustainable H_2 and CO_2: kinetic modeling, exergy analysis and techno-economic assessment

Moritz Herfet,[a+] Bruno Lacerda de Oliveira Campos,[a+] Túlio Franco Anacleto,[b] Gabriela Rodrigues Niquini,[a] Andréa Oliveira Souza da Costa,[b,c] Karla Herrera Delgado,[a] Stephan Pitter,[a] and Jörg Sauer [a]*

[a]Institute for Catalysis Research and Technology (IKFT), Karlsruhe Institute of Technologie (KIT), Hermann-von-Helmholtz-Platz 1, 76344 Eggenstein-Leopoldshafen, Germany.
[b]Departamento de Engenharia Química, Universidade Federal de Minas Gerais (UFMG), Av. Presidente Antônio Carlos 6627, Pampulha, 31270-901, Belo Horizonte, MG, Brazil.
[c]Departamento de Engenharia Mecânica, Universidade Federal de Minas Gerais (UFMG), Av. Presidente Antônio Carlos 6627, Pampulha, 31270-901, Belo Horizonte, MG, Brazil.

** Corresponding author. E-mail address: bruno.campos@kit.edu*
+ These authors contributed equally to this work.

Abstract

Dimethyl ether (DME) is a basic chemical, promising energy carrier and potential intermediate for chemical energy storage that can be produced from renewable hydrogen and captured CO_2, either indirectly (methanol synthesis followed by dehydration) or directly with both steps coupled in a single bifunctional reactor. In published comparisons, opinions differ as to which route is preferable, and it is well known to be sensitive to a number of assumptions: feedstock, flowsheet design, heat integration, cost model, and kinetics. This work contributes to a comparison in which several of these elements are strengthened simultaneously. High-pressure experiments over a $Cu/ZnO/ZrO_2$ + H-FER-20 catalyst bed, spanning 1200 h time on stream including 1320 operating points, were used to reparametrize a kinetic model, extending its validity to CO_2-rich feeds and representing the produced DME molar fractions with a mean relative error of 8 %. Both routes were simulated for an industrial large scale DME plant with detailed heat integration, including a water Rankine cycle, purge-gas combustion, and a two-stage refrigeration cycle for the cryogenic CO_2/DME separation. A cost model for a production capacity of 836.8 kton DME·a^{-1} for the location of Germany was developed. At this

Reaction Chemistry & Engineering Accepted Manuscript

configuration, both plants are fully self-sufficient in heat, in contrast to earlier reports. The direct route converts CO_2 with higher overall DME yield (95.3% vs. 91.7%), reducing purge losses, but its reactor is twice as large, owing to water inhibition, and the operation requires 21% more net electrical energy. On balance the trade-off favors the direct route, which reaches a higher overall exergy efficiency (87.1% vs 84.9%) and lower production costs (2195.4 vs 2234.9 €/t_{DME}, or 704.42 vs 743.97 €/t_{DME} on a conversion-cost basis) for hydrogen costs of 5300 €/t.

1. Introduction

The need to reduce CO_2 emissions in order to limit climate change has intensified global efforts towards the development and implementation of sustainable production of chemicals and fuels (1, 2). In this context, designing carbon-neutral or even carbon-negative pathways that integrate renewable resources and circular carbon strategies have become a central objective of current chemical engineering (3, 4).

Dimethyl ether (DME) has emerged as an attractive energy carrier and fuel (5-8), due to its high cetane number, significant volumetric energy density, and clean combustion characteristics. Furthermore, DME is widely used as an aerosol propellant, refrigerant, (9) and is also an important feedstock for the synthesis of olefins and other value-added chemicals (10-12). Finally, together with methanol, DME can serve as a central intermediate in the sustainable production of conventional liquid fuels (i.e. diesel, petrol, jet fuel) via olefin formation, oligomerization to tune the carbon chain length, and subsequent hydrogenation (10-12).

Industrially, DME is nowadays produced from methanol dehydration over a mild acidic catalyst, typically γ-Al_2O_3, at moderate temperatures (493 - 673 K) and low pressures (1 - 30 bar), resulting in a high single-pass conversion (70 - 85 %) (13). Methanol, in its turn, is produced commercially from syngas over a Cu/Zn-based catalyst, mostly $Cu/ZnO/Al_2O_3$, at moderate temperatures (523 - 573 K) and pressures (50 - 100 bar) (14). In Figure 1, the pathways from conventional and sustainable sources of $H_2/CO/CO_2$ to produce methanol and DME are illustrated.

Reaction Chemistry & Engineering Accepted Manuscript

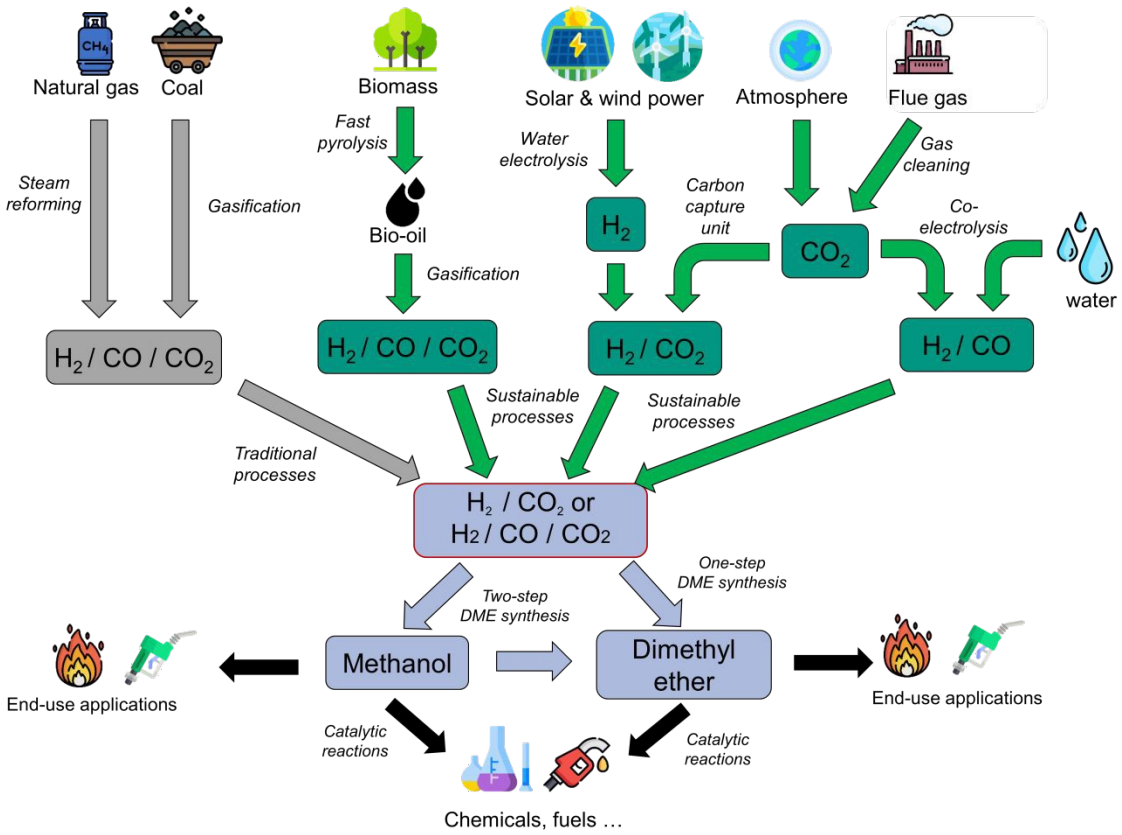


Figure 1. From H_2/CO/CO_2 sources to methanol and DME. Images: Flaticon, Freepik (15).

As methanol synthesis (R1 - R3) typically exhibits a lower single-pass conversion than methanol dehydration (R4), particularly when methanol is produced from H_2/ CO_2 feeds (16), many studies have explored integrating both steps in a single reactor (direct synthesis route). This is achieved by employing a bifunctional catalyst bed that simultaneously allows synthesis (R1 - R3) and dehydration (R4) of methanol in one reactor, thereby alleviating the equilibrium limitations of the methanol synthesis reaction (8, 13, 17-22). Recent work has progressed to demonstrate the feasibility up to the pilot-scale, by improving overall process efficiency (23-25).

$$CO + 2\,H_2 \rightleftharpoons CH_3OH \qquad \Delta H_{R\,(298K)} = -90.4\ kJ/mol \qquad (R1)$$

$$CO_2 + 3\,H_2 \rightleftharpoons CH_3OH + H_2O \qquad \Delta H_{R\,(298K)} = -49.4\ kJ/mol \qquad (R2)$$

$$CO + H_2O \rightleftharpoons CO_2 + H_2 \qquad \Delta H_{R\,(298K)} = -41.0\ kJ/mol \qquad (R3)$$

$$2\,CH_3OH \rightleftharpoons CH_3OCH_3 + H_2O \qquad \Delta H_{R\,(298K)} = -23.5\ kJ/mol \qquad (R4)$$

Reaction Chemistry & Engineering Accepted Manuscript

Generally, the direct route offers higher single-pass conversion, resulting in an enhanced overall yield of DME compared to the indirect route. It also features a simpler reaction-section layout, relying on a single reactor rather than two. On the other hand, the direct route demands a more complex downstream separation process - most notably the challenging cryogenic distillation required to separate CO_2 from DME. Therefore, comprehensive comparisons of the two process routes representing the industrial plant level are essential.

Several studies compared the costs of both process routes for varied feedstocks. Mevawala et al. studied the DME production from shale gas, and reported lower costs and better energy recovery for the indirect route (26). Bernardi et al. assumed syngas as feedstock, and reported similar performance of both routes in terms of costs, carbon and energy efficiencies (27). Nakyai et al. considered the product of biomass gasification as feedstock, and concluded that the direct route has significantly lower costs and exergy destruction (28).

To the best of our knowledge, only the works of Wu and Chien (22) and Dieterich et al. (18) conducted techno-economic analyses of both process routes for H_2/CO_2 as feedstock, i.e., derived from water electrolysis and carbon capture, allowing a reasonable comparison between the processes.

Wu and Chien (22) evaluated the conversion of CO_2 into DME based on direct and indirect synthesis (Methanol + DME based on reactive distillation) addressing also the techno-economic evaluation. For the direct DME synthesis they employed the kinetic model of Ateka et al. (17), which was developed for a physical catalyst mixture of Cu/ZnO/MnO and SAPO-18. The model was validated for 523 - 623 K, 10 - 40 bar, a space time of 1.25 - 20 $g_{cat} \cdot h^{-1} \cdot mol_C^{-1}$, H_2/CO_X molar ratios of 3 - 4, and CO_2/CO molar ratios of 0 - 1. Since the experimental data are based on a relatively short time on stream (30 h) accompanied by significant catalyst deactivation and non-negligible methane production, conclusions regarding a production process are limited.

Wu and Chien's research indicates that the implementation of a two-stage process can lead to a reduction in overall energy consumption and CO_2 emissions, provided that the liquid product is removed directly from the process. The implementation of reactive

Reaction Chemistry & Engineering Accepted Manuscript

distillation, incorporating side-stream distillation and heat integration (TSHI process), has the potential to further mitigate CO_2 emissions and energy consumption.

Dieterich et al. (18) compared different process routes for producing DME based on hydrogen and carbon dioxide: the direct (D-1) and indirect (I-1) DME synthesis, as well as the combination of these two processes with a pre-conversion of CO_2 into CO via the reverse water-gas shift reaction (rWGS) (direct: D-2 and indirect: I-2). The authors used the kinetic model of An et al. (29), which is based on Graaf's model (30, 31), to simulate the direct DME synthesis on [$Cu/ZnO/Al_2O_3/ZrO_2$]/HZSM-5, which was validated at temperatures between 483 and 543 K, pressures from 20 to 50 bar, and residence times between 1000 and 10000 $ml \cdot g_{cat}^{-1} \cdot h^{-1}$. However, there was no variation regarding feed composition (constant $H_2:CO_2$ = 3:1) reported.

Dieterich et al. (18) concluded that the direct DME synthesis without rWGS (D-1) has the lowest costs, closely followed by the indirect synthesis with rWGS (I-2).

In summary, it can be noted that the results from process comparisons are highly sensitive to several key assumptions, including the choice of feedstock, process flowsheets, kinetic models, cost models, heat integration strategy, and operating conditions explaining why the direct route is found to be superior in some studies, whereas the indirect route performs better in others.

When H_2/CO_2 was used as the feedstock, the applied kinetic models might be also limited by the issues described above, and Dieterich et al. (18) stated that the development of better kinetic models for the direct DME synthesis from H_2/CO_2 was an important aspect for further improvement. In addition, both Wu and Chien (22) and Dieterich et al. (18) reported the need for external heat supply for both process routes, indicating that the proposed heat integration strategies still offer considerable potential for improvement.

The present work comprises a multidisciplinary study aimed at comparing the direct and indirect routes for DME production from sustainable H_2 and CO_2. To ensure reliable kinetic modeling of the direct DME synthesis from H_2/CO_2, dedicated laboratory experiments were conducted with a broad range of operating conditions and refitting our previously developed kinetic model (32) using a new experimental database. Afterward, comprehensive process flowsheets were developed for both routes, incorporating detailed heat integration enabling thermal self-sufficiency. This was achieved taking into account

Reaction Chemistry & Engineering Accepted Manuscript

the implementation of a water Rankine cycle and a purge gas combustion section. In addition, the power requirements of the cryogenic distillation were rigorously calculated by designing a two-stage refrigeration cycle. The direct and indirect routes were subsequently evaluated and compared through energy, exergy, and techno-economic analyses.

2. Kinetic modeling

2.1 Direct DME synthesis

2.1.1 Kinetic experiments

Kinetic experiments of the direct DME synthesis were carried out in a multi-reactor-screening setup with six parallel stainless steel fixed bed reactors (inner diameter of 17.4 mm and a length of 600 mm).

The parallel test facility is comprised of four distinct mass flow controllers (MFC), which are utilized for the purpose of adjusting the feed gas compositions, which consist of $H_2/CO_2/CO/N_2$. All the gases used in the experiment (H_2 99.999 vol.% | CO 99.97 vol.% | CO_2/ N_2 50:50 ± 2 vol.% | N_2 99.9999 vol.%) were purchased from Air Liquide S.A.

The distribution of the synthesis gas stream to the respective reactors is adjusted by needle valves and quantified by mass flow meters (MFM). It is imperative that the volume flows of all reactors remain within a maximum deviation range of 1 %. Following the outlet of each reactor, a small volume flow of approx. 5 vol.% of the products is extracted via pneumatically actuated valves, which switch from reactor to reactor every 30 minutes. The volume flow of the feed gas is taken after the gas mixing station (comprising the four MFCs) by means of a solenoid valve and is directed to the measuring analysis line.

For the analysis of the feed and product gas, an FTIR CX 4000 from Gasmet Technologies Oy and an Inficon Micro GC Fusion gas chromatograph are employed. The micro-GC is equipped with two thermal conductivity detectors equipped with RT-Molsieve 5A, 0.25 mm (10 m) and RT-Q-Bond, 0.25 mm (12 m) columns.

The reactor pressure for the entire parallel laboratory plant is regulated by a Bronkhorst pressure controller placed at the end of the reactor configuration. To ensure proper

Reaction Chemistry & Engineering Accepted Manuscript

temperature control, each reactor has three adjustable heating zones (reactor head, reactor tube, reactor foot).

The dual catalytic system consisted of an in-house prepared $Cu/ZnO/ZrO_2$ (CZZ), active for the methanol synthesis, and a commercial zeolite H-FER-20 (FER) from Zeolyst International, active for the methanol dehydration to DME. Details regarding catalyst preparation and characterization of the in-house prepared $Cu/ZnO/ZrO_2$ (CZZ) are published by Polierer et al. (33) and Guse et al. (34, 35). Five reactors were loaded with different amounts of the catalyst mixture (1.1 g, 5.5 g, 11.0 g, 16.5 g, and 22.0 g, respectively) with a particle size of 250 - 500 µm, each maintaining a constant CZZ:FER ratio of 10:1. To prevent hot spots formation in the catalyst bed and to ensure isothermal conditions, the catalyst mixture was diluted with silicon carbide (SiC) at a constant SiC:[catalyst mixture] weight ratio of 5:1. For each reactor, 264 experimental data points under variable operating conditions were recorded, totaling 1320 points used for parametrization of the kinetic model. There were variations in pressure (30 - 50 bar), temperature (483 - 543 K), CO_2/CO_X ratio (0.25 - 1.00), and H_2/CO_X ratio (1.66 - 3.40). Full details on experimental plan are provided in Supplementary Information (SI, Section S1), and full experimental data is provided in Supplementary Information 2 (SI2).

2.1.2. Kinetic model development

The kinetic equations used in the plant simulations were based on the model published by Rodrigues Niquini et al. (32) for the direct DME synthesis. The parameters were refitted using the new experimental data, which particularly covers CO_2/CO_X = 1, aiming for a more accurate modeling of the production of DME from pure CO_2. The objective function to be minimized is given in Eq. 1 and consists of the weighted squared errors for the carbon-containing compounds.

$$\chi^2 = \sum_{k=1}^{N_P} \frac{\left(y_{CO}^k - \hat{y}_{CO}^k\right)^2}{{y_{CO}^k}^2} + \frac{\left(y_{CO_2}^k - \hat{y}_{CO_2}^k\right)^2}{{y_{CO_2}^k}^2} + \frac{\left(y_{CH_3OH}^k - \hat{y}_{CH_3OH}^k\right)^2}{{y_{CH_3OH}^k}^2} + \frac{\left(y_{DME}^k - \hat{y}_{DME}^k\right)^2}{{y_{DME}^k}^2} \quad \text{(Eq. 1)}$$

Reaction Chemistry & Engineering Accepted Manuscript

Here, y_i^k corresponds to the experimental molar fraction of component *i* in experiment *k*, $\hat{y}_i^k$ corresponds to the simulated value, and N_P is the number of experiments in the considered training set.

$$r_{CO_2hyd} = a_{CZZ} \cdot k_{CO_2hyd} \cdot \theta_a \cdot \theta_b \cdot {f_{H_2}}^{1.5} \cdot f_{CO_2} \cdot \left(1 - \frac{f_{CH_3OH} \cdot f_{H_2O}}{{f_{H_2}}^3 \cdot f_{CO_2} \cdot {K_{P,CO_2hyd}}^0}\right) \quad \text{(Eq. 2)}$$

$$r_{rWGS} = a_{CZZ} \cdot k_{rWGS} \cdot \theta_a \cdot \theta_b \cdot f_{CO_2} \cdot f_{H_2O} \cdot \left(1 - \frac{f_{CO} \cdot f_{H_2O}}{f_{H_2} \cdot f_{CO_2} \cdot {K_{P,rWGS}}^0}\right) \quad \text{(Eq. 3)}$$

$$r_{dehyd} = k_{dehyd} \cdot \theta_c \cdot {f_{CH_3OH}}^2 \cdot \left(1 - \frac{f_{DME} \cdot f_{H_2O}}{{f_{CH_3OH}}^2 \cdot {K_{P,dehyd}}^0}\right) \quad \text{(Eq. 4)}$$

The reaction rates (r_w) are given by Equations Eq. 2 - Eq. 4 (32), where a_{CZZ} represents the activity of the CZZ catalyst, k_w is the reaction constant of reaction w, θ_j is the fraction of free sites of type j, f_i is the fugacity of gas species i, and ${K_{P,w}}^0$ is the equilibrium constant of reaction w.

Equation Eq. 5 shows the calculation of the activity of the used catalyst depending on time on stream. In this case, we have chosen a reference time of 280 h, since the variations of operating conditions started during the following period (SI, Section S1). In this equation (Eq.5), k_d is the deactivation constant, to be fitted, and ToS is the time on stream.

$$a_{CZZ} = \frac{1}{1 + k_d \cdot (ToS - 280)} \quad \text{(Eq. 5)}$$

The coverage terms are given by Eq. 6 - 8 (32):

$$\theta_a = \left(1 + K_1 \cdot f_{CO_2} \cdot {f_{H_2}}^{0.5}\right)^{-1} \quad \text{(Eq. 6)}$$

$$\theta_b = \left(1 + K_2 \cdot f_{H_2O} \cdot {f_{H_2}}^{-0.5}\right)^{-1} \quad \text{(Eq. 7)}$$

$$\theta_c = \left(1 + K_3 \cdot f_{CH_3OH}\right)^{-1} \quad \text{(Eq. 8)}$$

The kinetic rate constants are given in the Arrhenius form, as described in Eq. 9:

Reaction Chemistry & Engineering Accepted Manuscript

$$k_j = A_j \cdot \exp\left(\frac{B_j}{T}\right) = A_j \cdot \exp\left(-\frac{E_{A,j}}{RT}\right) \quad \text{(Eq. 9)}$$

The equilibrium constants ${K_{P,CO_2hyd}}^0$, ${K_{P,rWGS}}^0$ and ${K_{P,dehyd}}^0$ are calculated using a three-parameter temperature function (36). The model has 9 parameters to be fitted: k_{CO_2hyd} (*A* and *B*), k_{rWGS} (*A* and *B*), k_{dehyd} (*A*), K_1, K_2, K_3 and k_d. As in previous works (32, 37, 38), the B term for k_{dehyd} was neglected, because it was shown to be not relevant statistically. Similarly, the temperature dependence in the site coverage terms K_{1-3} was also neglected, as in recent publications (37, 39-41). Following the approach of Slotboom et al. (40), the values of A for the kinetic rate constants were estimated in their logarithmic form, to improve numerical sensitivity.

To simulate the laboratory reactor, isothermal, isobaric and plug-flow conditions were assumed. The mass balance for each component *i* is given by Eq. 10, and the variation in the number of moles is given by Eq. 11 (32):

$$\frac{dy_i}{dz} = \frac{1}{L\dot{N}}\left[m_{CZZ} \cdot \left(\nu_{i,CO_2hyd} \cdot r_{CO_2hyd} + \nu_{i,rWGS} \cdot r_{rWGS}\right) + m_{FER} \cdot \nu_{i,dehyd} \cdot r_{dehyd}\right] - \frac{y_i}{\dot{N}} \cdot \frac{d\dot{N}}{dz} \quad \text{(Eq. 10)}$$

$$\frac{d\dot{N}}{dz} = -\frac{2 \cdot m_{CZZ} \cdot r_{CO_2hyd}}{L} \quad \text{(Eq. 11)}$$

Here, $\nu_{i,j}$ corresponds to the stoichiometric coefficient of component *i* in reaction *j*, L is the reactor length, $\dot{N}$ corresponds to the total molar flow, and m_{CZZ} and m_{FER} are the masses of Cu/ZnO/ZrO_2 and H-FER-20, respectively.

The parameter estimation was carried out in Matlab R2021busing the lsqnonlin method with default options for the minimization of the objective function (Eq. 1). The plug-flow differential equations for molar fractions and molar flow were integrated by the solver ode15s, using absolute and relative tolerances of 10^{-8}. To avoid divisions by zero in Eq. 2 - 4, the initial molar fractions for all components were set to a minimum value of $1 \cdot 10^{-7}$ (0.1 ppm).

2.2 Indirect DME synthesis

Reaction Chemistry & Engineering Accepted Manuscript

To simulate the reactions in the indirect DME synthesis, the model from Rodrigues Niquini et al. (42) was selected for CO_2 hydrogenation (R2) and the RWGS (R3), while the model from Bercic and Levec (43) was selected for the methanol dehydration to DME (R4).

2.2.1 Methanol synthesis model

Rodrigues Niquini et al. (42) developed a model for methanol synthesis based on the CZZ catalyst. The model was validated with 500 experimental points, which covered temperatures between 463 and 523 K, pressures between 30 and 60 bar and various H_2:CO_2 ratios, focusing on CO_2-rich conditions. The reaction rates for CO_2 hydrogenation (Eq. 2) and rWGS (Eq. 3) in $mol \cdot kg_{cat}^{-1} \cdot s^{-1}$ are as follows (Eq. 12 and Eq. 13):

$$r_{CO_2hyd} = a_{CZZ} \cdot k_{CO_2hyd} \cdot \theta_a \cdot f_{CO_2} \cdot f_{H_2}^2 \cdot f_{H_2O}^{-1} \cdot \left(1 - \frac{f_{CH_3OH} \cdot f_{H_2O}}{f_{H_2}^3 \cdot f_{CO_2} \cdot K_{P,CO_2hyd}^0}\right) \quad \text{(Eq. 12)}$$

$$r_{rWGS} = a_{CZZ} \cdot k_{rWGS} \cdot \theta_a \cdot f_{CO_2} \cdot f_{H_2}^{0.5} \cdot \left(1 - \frac{f_{CO} \cdot f_{H_2O}}{f_{H_2} f_{CO_2} \cdot K_{P,rWGS}^0}\right) \quad \text{(Eq. 13)}$$

The terms have the values given by Equations Eq. 14 - 17:

$$k_{CO_2hyd} = 3.4792 \cdot 10^5 \cdot \exp\left(-\frac{108880}{RT}\right) mol \cdot s^{-1} \cdot kg_{cat}^{-1} \cdot bar^{-2} \quad \text{(Eq. 14)}$$

$$k_{rWGS} = 4.7043 \cdot 10^{10} \cdot \exp\left(-\frac{135340}{RT}\right) mol \cdot s^{-1} \cdot kg_{cat}^{-1} \cdot bar^{-1.5} \quad \text{(Eq. 15)}$$

$$\theta_a = \left(1 + 0.1056 \cdot f_{CO_2} \cdot f_{H_2}^{0.5}\right)^{-1} \quad \text{(Eq. 16)}$$

$$a_{CZZ} = \frac{1}{1 + 5.673 \cdot 10^{-4} \cdot (ToS - 50)} \quad \text{(Eq. 17)}$$

In which the constant R has units of $J \cdot mol^{-1} \cdot K^{-1}$.

2.2.2 Methanol dehydration model

The kinetic model proposed by Bercic and Levec (43) for methanol dehydration to DME was originally developed for the γ-Al_2O_3 catalyst, and was validated for 563 - 633 K, 2.1 bar, and inlet concentrations of 15 - 90 mol.% methanol and 0 - 50 mol.% H_2O. In the present work, we use the apparent parameters proposed by the authors, considering intra-

Reaction Chemistry & Engineering Accepted Manuscript

particle heat and mass transfer limitations. The reaction rate (in $kmol \cdot kg^{-1} \cdot h^{-1}$) is given by Equation Eq. 18:

$$r_{dehyd} = \frac{k_{dehyd} \cdot K_M^2 \cdot \left(X_{CH_3OH}^2 - \frac{X_{DME} \cdot X_{H_2O}}{K_{P,dehyd}^0} \right)}{\left(1 + 2 \cdot \sqrt{K_M \cdot X_{CH_3OH}} + K_W \cdot X_{H_2O} \right)^4} \quad \text{(Eq. 18)}$$

The defined parameters with their values are given in Equations Eq. 19 - 21:

$$k_{dehyd} = 6.6 \cdot 10^8 \cdot \exp\left(-\frac{10800}{T}\right) kmol \cdot kg_{cat}^{-1} \cdot h^{-1} \quad \text{(Eq. 19)}$$

$$K_M = 7.2 \cdot 10^{-3} \cdot \exp\left(\frac{830}{T}\right) \%^{-1} \quad \text{(Eq. 20)}$$

$$K_W = 4.5 \cdot 10^{-3} \cdot \exp\left(\frac{1130}{T}\right) \%^{-1} \quad \text{(Eq. 21)}$$

For this reaction rate, the concentrations X_{CH_3OH}, X_{H_2O} and X_{DME} have units of mol%.

3. Process simulation

For both the direct and indirect synthesis routes, a DME synthesis plant from H_2/CO_2 with a production capacity of 104.6 ton·h^{-1} (or 837,000 ton·a^{-1}, for a workload of 8000 h·a^{-1}) was considered. This value was set based on the final production capacity target for the Haru Oni project, which aims to produce gasoline from renewable electricity and captured CO_2, with methanol and DME as intermediates (44), assuming 80% yield for the DME-to-gasoline step.

In the simulations, we consider that CO_2 feed at 298.15 K and 1.01325 bar is derived from carbon capture. The nature and amount of the typical impurities in CO_2 from carbon capture depend on the method – pre-combustion or post-combustion (45). The post-combustion method usually leads to higher CO_2 purities (> 99 %), and the main impurity is N_2, followed by water (46). For the calculations, a purity of 99.5 mol.% was assumed, with N_2 as secondary component. Hydrogen feed at 298.15 K and 1.01325 bar is considered to originate from water electrolysis (powered by renewable electricity) at the same purity of 99.5 mol.%. Although higher purities are feasible (47, 48), a more conservative scenario was chosen, allowing a proper simulation of inert accumulation in the chemical plant due to the recycle streams.

Reaction Chemistry & Engineering Accepted Manuscript

3.1 Process description – direct DME synthesis

The flowsheet of the direct DME synthesis plant considered in this work follows the approach of Dieterich et al. (18) regarding downstream: an absorption column with water and methanol followed by three distillation columns. However, in this work, the flowsheet design was significantly enhanced with a detailed heat integration simulated in Aspen Plus, which included three auxiliary sections: a water Rankine cycle, a furnace for purge combustion, and a two-stage refrigeration cycle. The flowsheet is provided in Figure 2.

Feed CO_2 and H_2 are separately compressed to 50 bar in three and four stages, respectively, with intermediate cooling. The reactants and the recycle streams are mixed, pre-heated to 493 K, and enter the DME reactor, a shell-and-tube equipment with the catalyst bed on one side, and boiling water at 523 K as cooling fluid on the other side. The product stream is step-wise cooled to 303.15 K for heat recovery and enters an absorption column, where each, water, methanol, and DME nearly completely as well as 45 % of CO_2 are recovered in the liquid phase. The gas stream is recompressed and recycled, while the liquid stream is depressurized to 10 bar, heated to 338 K and enters the first distillation column (COL1-CO2). Vapor CO_2 leaves the column top at 233 K, is recompressed to 50 bar, heated and recycled. A mixture of DME, water and methanol leave the column bottom as liquid. This mixture is depressurized to 8 bar and enters the second distillation column (COL2-DME), where liquid DME at > 99.5 wt.% purity is obtained on the top and a water-methanol mixture exits the column bottom. The water-methanol mixture is split into two streams: one stream is depressurized to 1 atm and enters the distillation column (COL3-MET), where methanol and water are separated; the other stream is cooled and pumped to the absorption column to serve as absorbent. After the last distillation column (COL3-MET), liquid water leaves the plant while liquid methanol is pumped back and recycled.

Reaction Chemistry & Engineering Accepted Manuscript

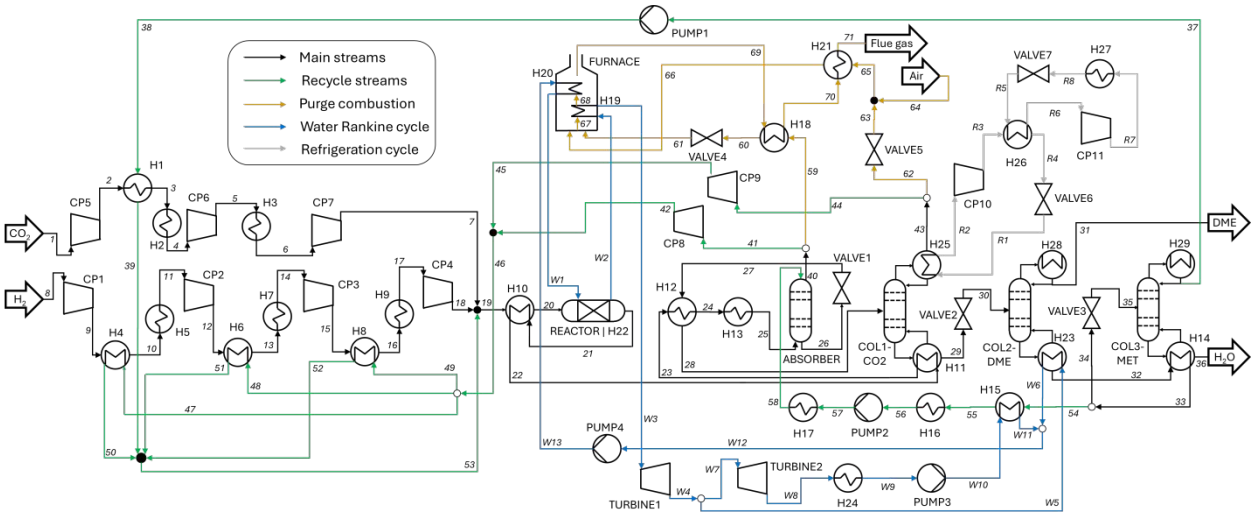


Figure 2. Flowsheet of the direct route of the DME synthesis.

To avoid the accumulation of inert material in the plant, a fraction (2%) of the outlet gas streams from the absorber and the first distillation column (COL1-CO2) are purged. The purge streams are preheated and burned in a fired heater. The heat of combustion is recovered, and the flue gas exits the plant.

To make use of the purge combustion heat and the reaction enthalpy of the DME synthesis, a water Rankine cycle was proposed. Saturated water (stream W1) at 523 K enters the reactor as cooling fluid and is completely evaporated, recovering the heat of reaction. Saturated steam is further heated in the furnace, and superheated steam does work in the first turbine until 6.6 bar. This pressure was chosen so that the resulting stream has a condensation temperature of 10 K higher than the temperature of the reboiler of the DME distillation column (COL2-DME), so that it is used as a heat source in this equipment. The turbine flow at the outlet is divided into two streams: stream W5 provides heat to COL2-DME, while stream W7 does work in a second turbine until 0.6 bar. This pressure was chosen so that vapor fraction in the outlet stream is higher than 0.93, protecting the turbine against erosion (49). The outlet stream is fully condensed, pumped to 6.6 bar, recovers some heat, and is directly mixed with stream W6. The resulting stream is pumped to 40.8 bar and heated in the furnace until the boiling temperature (523 K), completing the cycle.

To remove heat from the condenser of the first distillation column (COL1-CO2) at 233 K, a two-stage refrigeration cycle was designed. CO_2 is the working fluid of the colder cycle

Reaction Chemistry & Engineering Accepted Manuscript

and ammonia is the working fluid of the warmer cycle. In each cycle, a liquid-gas mixture exits the expansion valve and removes heat from the cold source until complete evaporation. The vapor is compressed and delivers heat to the hot source, until complete condensation. Finally, the pressure is reduced in a valve, and partial evaporation occurs, cooling the fluid and closing the cycle.

The operating temperatures of the heat exchanger (H27) connecting the stages in the refrigeration cycle were determined by maximizing its global performance coefficient (β_{RC}, Eq. 22) (see Figure 3).

$$\beta_{RC} = \dot{Q}_{H25}/(\dot{W}_{CP11} + \dot{W}_{CP12}) \quad \text{(Eq. 22)}$$

Q_{H25} is the heat which is removed from the condenser of COL1-CO2, and $\dot{W}_{CP,i}$ is the compression power of compressor i.

Between 250 and 260 K, there is a plateau in the performance coefficient of the cycle, as the increase in the CO_2 compression power compensates for the decrease in NH_3 compression power. The temperature of 256.15 K was selected for stream R4 (CO_2 outlet), while the corresponding stream R5 temperature (NH_3 inlet) was 245.7 K chosen to ensure the 10 K minimum temperature approach.

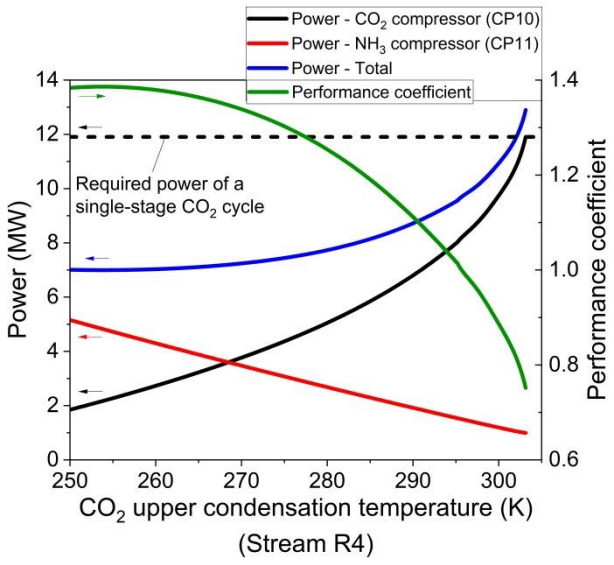


Figure 3. Power consumption and performance coefficient of the two-stage refrigeration cycle vs. CO_2 upper condensation temperature (stream R4).

Reaction Chemistry & Engineering Accepted Manuscript

3.2 Process description – indirect DME synthesis

The flowsheet of the indirect process is shown in Figure 4. Feed CO_2 is mixed with a recycle stream and compressed to 50 bar in three stages, with intermediate cooling and intermediate phase separation (small condensed amounts of methanol and water). H_2 is compressed to 50 bar in four stages. The reactants and the recycle streams are mixed, pre-heated to 493 K, and enter the methanol reactor (REACTOR1), a shell-and-tube equipment with the catalyst bed in one side, and boiling water at 523 K as cooling fluid in the other side (similarly to the direct DME synthesis reactor). The product stream is cooled down to 303.15 K in several steps for heat recovery and enters a flash drum (FLASH1), where H_2, CO, N_2 and most CO_2 leave the plant as gases. This gas stream is recompressed and recycled, while the liquid stream is depressurized to atmospheric pressure and enters the second flash drum (FLASH2), where further CO_2 is removed as vapor. This CO_2-rich vapor stream is mixed with feed CO_2 before recompression to 50 bar. The liquid stream from the second flash, i.e. crude methanol, is mixed with a water-methanol recycle stream from the methanol dehydration section and enters the methanol distillation column (COL1-MET). Water leaves the column at the bottom, methanol at high purity leaves the column at the top as liquid distillate, and a small stream containing methanol and CO_2 leaves the top of the column as vapor distillate and is recycled.

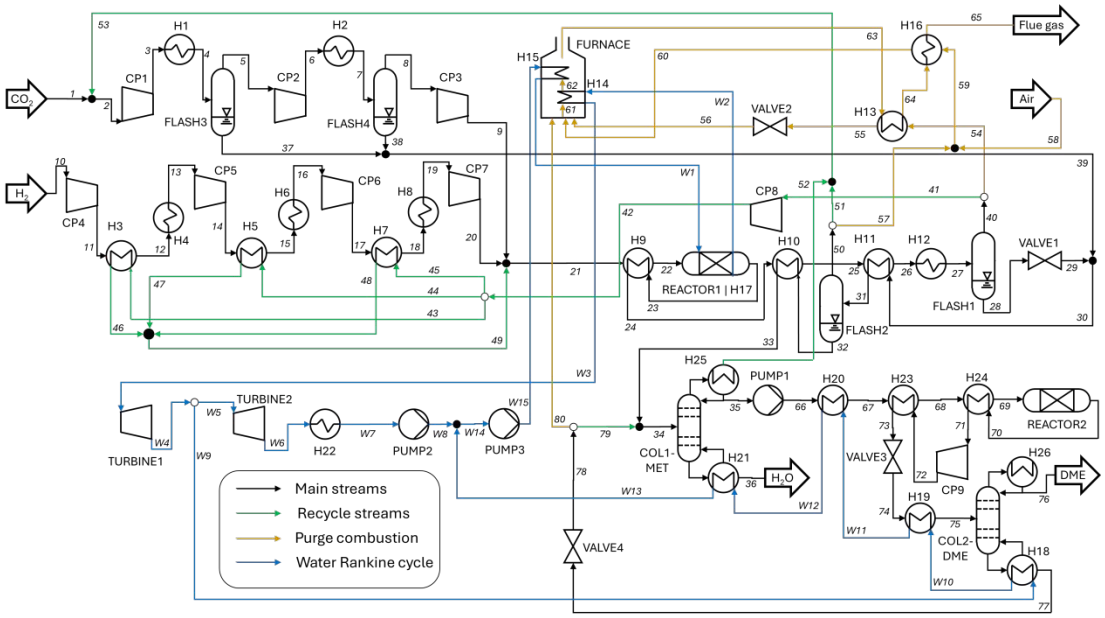


Figure 4. Flowsheet of the indirect DME synthesis.

Reaction Chemistry & Engineering Accepted Manuscript

In the methanol dehydration section, methanol is compressed to 15 bar, heated to 553 K in several steps, and enters the methanol dehydration reactor (REACTOR2), which is operated in adiabatic mode. The product stream is at a temperature of 680 K and is used to heat the reactant stream in two steps (H23 and H24), with a compressor in between (CP9) to pressurize the product to 23.5 bar to increase the dew point and improve utilization of the condensation enthalpy of the product.

The product stream is depressurized to 8 bar, heated to 375 K and enters the DME distillation column (COL2-DME), where liquid DME at > 99.5 wt.% purity is obtained at the top and a water-methanol mixture exits the column bottom. The latter is depressurized to 1.01325 bar and enters the methanol distillation column (COL1-MET), after mixing with the crude methanol stream from the methanol synthesis.

Similarly to the direct DME synthesis, a fraction (2%) of the outlet gas streams from the flash drums are purged, preheated and burned in a fired heater. The heat of combustion is recovered, and the flue gas exits the plant.

A water Rankine cycle is also proposed, similar to the direct DME synthesis. Saturated water (stream W1) at 523 K enters the methanol reactor as cooling fluid and is completely evaporated, recovering the heat of reaction. Saturated steam is further heated in the furnace, and superheated steam does work in the first turbine until 1.53 bar. This pressure was chosen so that the resulting stream has a condensation temperature of at least 10 K higher than the temperature of the reboiler of the methanol distillation column (COL1-MET), allowing it to be used as a heat source in this equipment. The outlet turbine stream is split into two: stream W9 provides heat to each column reboilers as well as two heat exchangers (H20 and H21), while stream W5 does work in a second turbine down to 0.05 bar. This pressure was selected to get a condensation temperature of the outlet stream higher than 303 K, so that it can be fully condensed by cooling water (considered at 293 K). The outlet stream is fully condensed, compressed to 1.53 bar, and is directly mixed with stream W13. The resulting stream is compressed to 40.8 bar and heated in the furnace until its boiling temperature (523 K), completing the cycle.

Reaction Chemistry & Engineering Accepted Manuscript

3.3 Flowsheet simulation with Aspen Plus

Simulation of both processes was performed with Aspen Plus V12, and the flowsheet figures simulated are provided in the Supplementary Information 2 (SI2). Two material property estimation methods were used for the main streams: SRK for higher pressures ($p > 10$ bar) and NRTL for lower pressures ($p \leq 10$ bar). For the water Rankine cycle, which consists of pure water streams, IAPWS-95 was selected, which is the standard method for liquid water and steam. For the pure CO_2 and NH_3 streams of the refrigeration cycle, REFPROP was selected, which is the standard database for refrigerant fluids.

To simulate the reactors of the direct DME synthesis, the methanol synthesis, and the methanol dehydration to DME, the RPLUG unit was used. The kinetic models described in Sections 2.1.2 and 2.2 were implemented as Langmuir-Hinshelwood-Hougen-Watson (LHHW) reaction models.

For the kinetic models of the direct DME synthesis and the methanol synthesis, which have a time-dependent activity term (a_{CZZ}), the activity coefficient correspondent to a time-on-stream of 280 h was set for both cases. The incorporation of the activity term, a_{CZZ}, in the kinetic models was motivated by the observation of catalyst deactivation during the experimental procedures, as reflected in the measurements of reference points. This approach was undertaken to enhance the accuracy and precision of the kinetics, thereby ensuring more precise and reliable results for improving the kinetic fit. It should be emphasized that these functions probably lead to underestimations of the catalyst lifetime, because no reported stabilizers and promoters are also added to the formulation of industrial methanol catalysts to improve the material stability and shelf life.

Both, the direct DME synthesis and the methanol synthesis process were simulated utilizing multitube reactors with a constant cooling at 523 K, and the global heat transfer coefficients were estimated with a method from literature (50, 51), which was also described in detail in a previous work (16). Since the catalyst bed consists mostly of the methanol catalyst, pure methanol catalyst was considered in the calculations of the heat transfer coefficients.

Reaction Chemistry & Engineering Accepted Manuscript

The catalyst densities were set to:

- For $Cu/ZnO/ZrO_2$ (CZZ, methanol synthesis): ρ_{CZZ} = 1200 kg m^{-3} (value from $Cu/ZnO/Al_2O_3$ tablets (52), which should be relatively close to the density of $Cu/ZnO/ZrO_2$ tablets)
- For the zeolite H-FER-20 (FER, methanol dehydration in the direct DME synthesis): ρ_{FER} = 500 kg m^{-3} (value of 415 kg m^{-3} for small particles (37) + 20% rough estimation of density increase due to tableting)
- For γ-Al_2O_3 (methanol dehydration in the indirect DME synthesis): $\rho_{\gamma\text{-}Al2O3}$ = 882 kg m^{-3} (53)

In the direct DME synthesis, the catalyst bed consisted of 95 wt.% of CZZ and 5 wt.% of H-FER-20, following the recommendations of a previous study that optimized the catalyst bed composition (37). The density of the dual catalyst bed was set to ρ_{bed} = 1121.5 kg m^{-3}, which is a weighted average value.

Since thermodynamics of the methanol dehydration is favorable for DME production and is less dependent on temperature, a high single pass conversion of approx. 80% can be reached with an adiabatic reactor. Therefore, the methanol dehydration was simulated as an adiabatic reactor, simplifying the process and lowering costs (compared to a tube-shell multitube reactor).

The fired heater was simulated with the RGIBBS unit, which considers that chemical equilibrium is achieved when the free Gibbs energy of the system is minimized. Air excess was set to 15% (54).

Some heat exchangers were simulated with the HeatX unit in counter-current flow. However, to facilitate flowsheet convergence and to allow heat transfer to the distillation columns, most heat exchangers were simulated with two Heater units linked with a heat stream: one Heater unit simulates cooling (excl.: H3-COOL) while the other unit simulates heating (excl.: H3-WARM). A general minimum temperature approach of 10 K was applied (directly set for HeatX units and checked afterwards for Heater units), and 25 K was considered for the heat exchangers related to the purge combustion.

Reaction Chemistry & Engineering Accepted Manuscript

The compressors were modeled with the ASME method, considering adiabatic operation, a mechanical efficiency of 0.95, and an isentropic efficiency of 0.80 (55). The turbine was also simulated with the ASME method, considering adiabatic operation, a mechanical efficiency of 0.95, and an isentropic efficiency of 0.92 (56). Adiabatic operation and an efficiency of 0.70 was assumed for the pumps (57).

The distillation columns and the absorber were simulated with the rigorous RadFrac model, with a Murphree efficiency of 0.75 set to all intermediate stages (58, 59).

Heat losses of all equipment to the environment were neglected. The relative tolerance of all equipment calculations was set to 10^{-5}. Flowsheet convergence was achieved through the Broyden method with a relative tolerance of 10^{-4}, which corresponds to a mass balance closure of 99.99%.

3.4 Exergy analysis

Exergy is a thermodynamic property derived from combining the First and Second Laws, meaning it explicitly accounts for entropy generation in addition to energy conservation. Because of this, exergy is not conserved during real processes (unlike energy). Any real process produces entropy, and the entropy generation reduces the portion of energy that can be converted into useful work. The impact of entropy generation appears in the analysis as exergy destruction, and they are directly proportional (60).

For a steady-state process, the exergy balance can be defined as follows (61).

$$\sum_{i=1}^{N_{in}} \left(\dot{m}_{i,in} \cdot e_{j,in}\right) - \sum_{i=1}^{N_{out}} \left(\dot{m}_{i,out} \cdot e_{j,out}\right) + \sum_{i=1}^{n} \dot{Q}_i \left(1 - \frac{T_0}{T_i}\right) - \dot{W} = E_{D,k} \qquad \text{(Eq. 23)}$$

Where $\dot{m}_i$ is the mass flow rate of current i, e_j is the specific exergy flow i, N_{in} is the number of streams entering the unit, N_{out} is the number of streams leaving the unit, $\dot{Q}_i$ is the heat rate transferred from the system to the surroundings ($i = 1...n$) other than the environment, $\dot{W}$ is the work performed by the fluid and $E_{D,k}$ is the exergy destruction of a process k. Note that the two first terms of the balance represent exergy related to the mass flow and the third term is the exergy related to the heat rate.

The specific exergy flow has two contributions (Eq. 24): physical exergy ($e_{j,phy}$) and chemical exergy ($e_{j,ch}$) (62). The physical exergy represents the maximum useful work

Reaction Chemistry & Engineering Accepted Manuscript

obtainable as a stream is brought from its initial state to the environmental temperature and pressure. In contrast, the chemical exergy assumes the stream is already at the environment's temperature and pressure. It measures the work potential associated with the chemical differences between the stream and the reference environment, commonly called the dead state. In essence, chemical exergy reflects the departure of the stream's composition from chemical equilibrium with the environment (63).

$$e_j = e_{j,phy} + e_{j,ch} \quad \text{(Eq. 24)}$$

The physical exergy is calculated as follows (61).

$$e_{j,phy} = \left(h_j - h_j^0\right) - T_0\left(s_j - s_j^0\right) \quad \text{(Eq. 25)}$$

Here h_j is the specific enthalpy, s_j is the specific entropy, h_j^0 and s_j^0 are the specific enthalpy and entropy at reference conditions (298.15 K and 1.01325 bar), T_0 is the reference temperature (298.15 K).

Chemical exergy values depend on the composition of the environment (64). Szargut defined the environmental air as reference for gases, the sea composition as reference for liquids and the lithosphere as reference for solids (64). In Table 1, values of standard chemical exergy are provided. Except for DME and methanol, all values were taken from Szargut (65). Equations Eq. 26 and Eq. 27 were used to predict the molar chemical exergy of DME and methanol respectively ($e_{j,ch}$), considering complete combustion as the basis for the calculations (49).

$$e_{DME,ch} = -\Delta G_{0,reaction} - 3e^0_{O_2,ch} + 2e^0_{CO_2,ch} + 3e^0_{H_2O,ch} \quad \text{(Eq. 26)}$$

$$e_{MeOH,ch} = -\Delta G_{0,reaction} - 1.5e^0_{O_2,ch} + e^0_{CO_2,ch} + 2e^0_{H_2O,ch} \quad \text{(Eq. 27)}$$

$e_{i,ch}$ is the predicted standard chemical exergy of component i, $e^0_{j,ch}$ is the standard chemical exergy of component j, and $\Delta G_{0,reaction}$ is the Gibbs energy of the respective complete combustion reaction.

Reaction Chemistry & Engineering Accepted Manuscript

Table 1. Standard Chemical Exergy by substance. Values were taken from (65), except those from DME and methanol, which were estimated.

Substance	Standard Chemical Exergy (kJ/mol)
CO	275.10
CO_2	19.87
DME	1417.95
H_2	236.09
H_2O	0.90
MeOH	717.63
N_2	0.72
NH_3	337.90
O_2	3.97

Exergy analysis was performed for the global process as well as for the various sections of the plant (see Section S5 in the SI for details). The exergy efficiency of each process ($\eta_{Ex,i}$) is calculated as follows (66):

$$\eta_{Ex,i} = \sum_{i=1}^{n} \dot{Ex}_{out,i} / \sum_{i=1}^{m} \dot{Ex}_{in,i} \quad \text{(Eq. 28)}$$

$\dot{Ex}_{in,i}$ is the process inlet exergy stream i (inlet flows, power consumption, heat consumption), and the $\dot{Ex}_{out,i}$ is the outlet exergy stream i (outlet flows, power generation, heat delivered to other process). The exergy of the flows discarded in the environment (e.g., flue gas, water) is considered lost exergy and is not accounted in $Ex_{out,i}$.

The exergy efficiency of the global process (η_{Ex}) is calculated as follows (67):

$$\eta_{Ex} = \frac{\dot{m}_{DME} \cdot e_{DME}}{\dot{m}_{H_2} \cdot e_{H_2} + \dot{m}_{CO_2} \cdot e_{CO_2} + P_{el} + E_Q} \quad \text{(Eq. 29)}$$

Here, P_{el} is the total net required electric power, and E_Q is the total exergy input associated with heat demand, since both processes are self-sufficient in terms of heat, $E_Q = 0$.

3.5 Costs estimation

In this work, the considered plant capacity for both process routes is 836.8 kton DME·a^{-1}. For the economic evaluation of this industrial DME process comparison, it is necessary to calculate the capital expenditures (CAPEX) and operational expenses (OPEX) to get the

Reaction Chemistry & Engineering Accepted Manuscript

net production costs (NPC) for a DME production in Germany. Flowsheet data was taken from Aspen Plus, and the cost estimation was calculated as described in this section.

3.5.1 Capital expenditures (CAPEX)

The estimation of equipment costs is done with the factorial method, where, a and b are constants derived from previous projects, S is the size parameter, and n is the scaling factor (57, 68, 69).

$$C_e = a + b \cdot S^n \quad \text{(Eq. 30)}$$

The essential data necessary for estimating the costs of the equipment varies depending on the equipment group. The domains of application for the variables employed are delineated in the calculation formula (57). In instances where the equipment exceeds the specified scope, it was presumed that the costs would be estimated through extrapolation, contingent on the equipment's dimensions. For this purpose, Eq. 30 from Towler et al. is used, which describes the capital costs (C_1, C_2) as a function of capacity (S_1, S_2). For methanol plants, which have high amounts of mechanical work, an exponent of 0.8 is used, compared to an exponent of 0.6 (six-tenths rule) generally used for the chemical industry.

$$C_2 = C_1 \cdot \left(\frac{S_2}{S_1}\right)^n \quad \text{(Eq. 31)}$$

The cost estimate for the equipment in this case refers to carbon steel, meaning that no additional material factor needs to be taken into account for the estimate. The material utilized in the fabrication of the component exhibits resistance to reaction pressure, reaction temperature, and the substances employed during the manufacturing process.

The costs estimation of the distillation columns is determined with reference to the cost of pressure vessels, packaging, and trays, as described in Towler et al. (57). The detailed calculation methodology can be found in the SI (Section S2).

The costs of the reactors of methanol and direct DME synthesis were calculated using the methodology for heat exchangers, as the reactors operate like shell and tube heat exchanger. According to Peters et al. (68), this is a frequently made assumption in the context of tube bundle reactors. It was considered that the tube side is filled with the

Reaction Chemistry & Engineering Accepted Manuscript

catalyst material, while the cooling fluid flows on the shell side. The dehydration reactor is a typical pressure vessel with an inlet and outlet connection.

The cost functions from Towler et al. (57) are associated with the U.S. Gulf Coast in January 2010. They were converted to the level of June 2024 using the Chemical Engineering Plant Cost Index (CEPCI) (see Eq. 32).

$$C_{e,i}^{2024,June} = C_{e,i}^{2010,January} \cdot \frac{\mathrm{CEPCI}_{2024,\,\mathrm{June}}}{\mathrm{CEPCI}_{2010,\,\mathrm{January}}} \quad \text{(Eq. 32)}$$

Where $C_{e,i}^{X}$ is the cost of equipment i at the date X, $\mathrm{CEPCI}_{2024,\ \mathrm{June}}$ = 798.8 (70), and $\mathrm{CEPCI}_{2010,\ \mathrm{January}}$ = 532.9 (57). The equipment costs for June 2024 were determined in euros using currency conversion and the average exchange rate (1 EUR = 1.0759 USD) of June 2024.(71) The fixed capital investment costs consist of direct costs (C_{DC}) and indirect costs (C_{IC}), which can be calculated using appropriate factors. The factors employed for subsequent calculations are derived from the work of Peters et al.(68), and are provided in the Section S3 of the SI. The fixed capital investment (FCI) costs were estimated in accordance with the established equation (see Eq. 32). The total capital investment (TCI) includes fixed capital investment and the working capital (WC), defined as 10% of the TCI (Eq. 34).

$$FCI = C_{DC} + C_{IC} = \left(\sum_{i}^{7} f_{DC,i}\right) \cdot \left(\sum_{i}^{5} f_{IC,i}\right) \cdot \left(\sum_{i}^{n_{EQ}} C_{e,i}^{2024,June}\right) \quad \text{(Eq. 33)}$$

$$TCI = FCI + WC = \frac{FCI}{0.90} \quad \text{(Eq. 34)}$$

The annuity method is a financial tool employed to calculate the annual capital costs (ACC) (72), which encompasses both the fixed capital costs and the working capital. The following assumptions were made: plant life of 20 years (N), 10% interest rate (i), no salvage value.

$$ACC_{FCI} = FCI \cdot \frac{i \cdot (1+i)^N}{(1+i)^N - 1} \quad \text{(Eq. 35)}$$

$$ACC_{WC} = WC \cdot i \quad \text{(Eq. 36)}$$

$$ACC = ACC_{FCI} + ACC_{WC} \quad \text{(Eq. 37)}$$

Reaction Chemistry & Engineering Accepted Manuscript

3.5.2 Operating expenses (OPEX)

Operating expenses (OPEX) are classified into two categories, direct and indirect OPEX:

- Direct costs encompass, for instance, feedstock expenses, energy expenditures, and catalyst costs, which are dependent on the plant production rate, as these costs are directly associated with material and energy flows.
- Indirect costs, including operating labor, administrative expenses, and maintenance costs, are independent of the plant production rate.

Table 2 provides a list of reference prices that were considered in the determination of direct OPEX. In Section S4 of the SI, the methodology to estimate the indirect OPEX is provided, including the operating labor.

Table 2. Costs of direct OPEX.

Item	Price (€/unit)	unit	Reference
Hydrogen (H_2)	5,300	ton	(73)
Carbon-dioxide (CO_2)	51.96	ton	(74)
Electricity	0.1047	kWh	(75)
Cooling water	0.00125	ton	(72)
Clean water replacement	2	ton	(72)
Methanol catalyst ($Cu/ZnO/ZrO_2$)	20,951.4	ton	(76)
Dehydration catalyst (γ-Al_2O_3)	22,275.6	ton	(76)
Total Organic Carbon (TOC) abatement of process water	1,938	ton C	(77)

3.5.3 Net production costs (NPC)

The net production costs were calculated as costs per year (Eq. 38) and per kg of product (Eq. 39). This approach considers the calculated annual capital costs (ACC), direct operational expenses ($OPEX_{dir}$), indirect operational expenses ($OPEX_{ind}$), and total DME production rate ($\dot{m}_{DME}$).

$$NPC\left(\frac{€}{a}\right) = ACC + OPEX_{dir} + OPEX_{ind} \quad \text{(Eq. 38)}$$

$$NPC\left(\frac{€}{kg}\right) = \frac{ACC + OPEX_{dir} + OPEX_{ind}}{\dot{m}_{DME}} \quad \text{(Eq. 39)}$$

4. Results

Reaction Chemistry & Engineering Accepted Manuscript

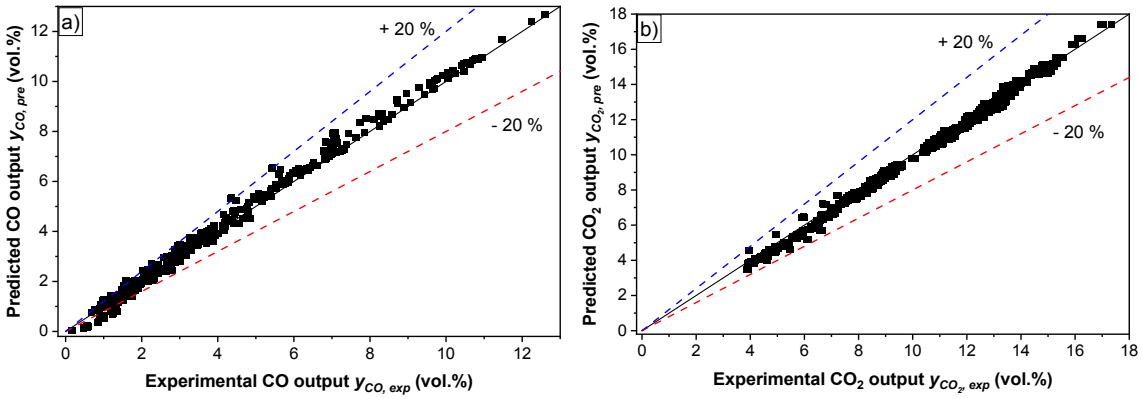
4.1 Kinetic modeling

Full experimental data of the direct DME synthesis were successfully conducted and are provided in the Supplementary Information 2 (SI 2). After performing the 5-fold cross-validation procedure (78), the parameter set with the lowest overall χ^2 is given in Table 3.

Table 3. Estimated parameters within the chosen training set.

Parameter		Value ± 95% CI		Unit
$\boldsymbol{k_{CO_2hyd}}$	$\ln A$	16.24 ± 0.23	$k_{CO_2hyd} = 1.130 \cdot 10^7 \cdot \exp\left(-\frac{102030}{RT}\right)$	$mol \cdot s^{-1} \cdot kg_{cat}{}^{-1} \cdot bar^{-2.5}$
	B	$(-12.272 \pm 0.058) \cdot 10^3$		
$\boldsymbol{k_{rWGS}}$	$\ln A$	29.98 ± 0.44	$k_{rWGS} = 1.052 \cdot 10^{13} \cdot \exp\left(-\frac{136400}{RT}\right)$	$mol \cdot s^{-1} \cdot kg_{cat}{}^{-1} \cdot bar^{-2}$
	B	$(-16.40 \pm 0.21) \cdot 10^3$		
$\boldsymbol{k_{dehyd}}$	$\ln A$	3.04 ± 0.30		$mol \cdot s^{-1} \cdot kg_{cat}{}^{-1} \cdot bar^{-2}$
K_1	A	0.0833 ± 0.0062	$K_1 = 0.0833$	$bar^{-1.5}$
$\boldsymbol{K_2}$	A	147 ± 22	$K_2 = 147$	$bar^{-0.5}$
$\boldsymbol{K_3}$	A	59 ± 31	$K_3 = 59$	bar^{-1}
$\boldsymbol{k_d}$		$(5.682 \pm 0.093) \cdot 10^{-4}$	$k_d = 5.682 \cdot 10^{-4}$	h^{-1}

The parity plots for the carbon-containing compounds are shown in Figure 5. The simulated molar fractions usually differ from the experimental values by less than 20% with respect to the experimental values: 97% of the CO values, 100% of the CO_2 values, 92% of the methanol values and 94% of the DME values are within this range.



Reaction Chemistry & Engineering Accepted Manuscript

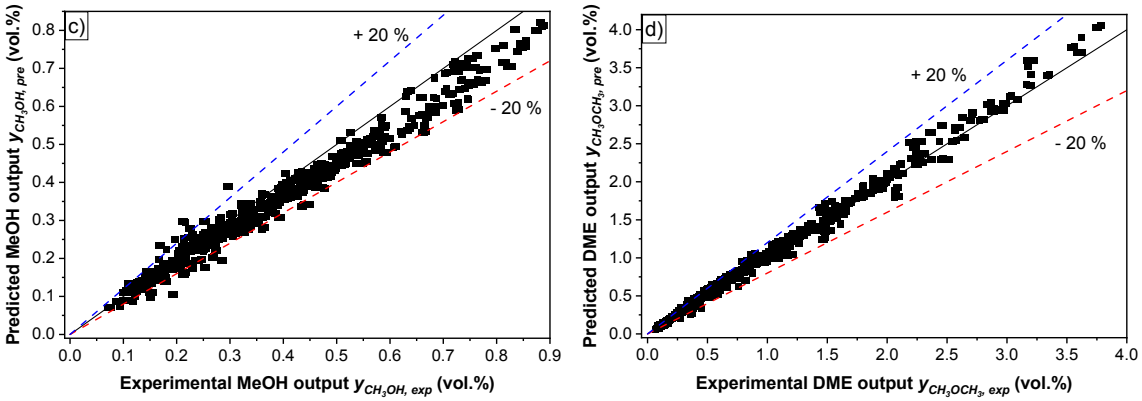


Figure 5. Parity plots of the carbon-containing compounds: predicted vs. experimental output concentrations: a) CO, b) CO_2, c) MeOH, d) DME.

The normalized mean squared error and the mean relative error for a component j were calculated as follows:

$$MSE_{norm\,j} = \frac{1}{N_P}\sum_{i=1}^{N_P}\frac{\left(y_{j,out}^{i} - \hat{y}_{j,out}^{i}\right)^2}{{y_{j,out}^{i}}^2} \qquad \text{(Eq. 40)}$$

$$MRE_j = \frac{100\%}{N_P}\sum_{i=1}^{N_P}\frac{\left|y_{j,out}^{i} - \hat{y}_{j,out}^{i}\right|}{y_{j,out}^{i}} \qquad \text{(Eq. 41)}$$

The errors for the carbon-containing compounds, i.e., CO, CO_2, methanol and DME, are shown in Table 4.

Table 4. Objective function and error indicators of the model.

Statistic	Training	Validation	Training + Validation
χ^2	35.08	8.82	43.90
MSE_{norm} x 10^3 – CO	5.87	4.67	5.63
MSE_{norm} x 10^3 – CO_2	0.97	0.90	0.95
MSE_{norm} x 10^3 – CH_3OH	16.15	15.97	16.11
MSE_{norm} x 10^3 – DME	10.44	11.33	10.62
MRE (%) – CO	4.26	3.89	4.19
MRE (%) – CO_2	2.05	1.81	2.01
MRE (%) – CH_3OH	10.68	10.64	10.67

Reaction Chemistry & Engineering Accepted Manuscript

MRE (%) – DME	7.86	8.25	7.94

Differences between the statistics for the training and validation sets are not significant, highlighting the capability of the model to predict values outside the training set range. Moreover, the mean relative errors for DME predictions are around 8%, indicating the model's accuracy to predict the experimental data.

4.2 Process simulation

Flowsheet simulations of the direct and the indirect routes were successfully simulated in Aspen Plus, with both plants producing 104.6 ton h^{-1} of DME at high purity (> 99.5 wt.%). In the Supplementary Information 3, the properties of all streams of the direct route are provided, as well as the design parameters, operating conditions, and output parameters of all equipment. In Supplementary Information 4, analogous results are provided for the indirect route.

In Table 5, a summary of the reactor configuration details is provided. The required size of the direct DME synthesis reactor to reach a CO_2 single-pass conversion close to equilibrium is double the size compared to the methanol synthesis reactor (see Figure 6). The reaction rates of both processes are similar until approx. 17% CO_2 conversion, which is the region of "fast kinetics". At higher CO_2 conversion, the reaction rates of both processes slow down significantly, especially the methanol synthesis, due to its proximity to the equilibrium (at approx. 23%). The direct DME synthesis continues from 17 % to 32% of CO_2 single-pass conversion at much slower reaction rates ("slow kinetics region") compared to the beginning, requiring a large catalytic bed (12x higher than the region of "fast kinetics"). Since the CO_2 conversion at 17% is still far from the thermodynamic equilibrium in the direct DME synthesis, the reaction rates of CO_2 consumption are predominantly constrained by water inhibition. This phenomenon is characterized by the attainment of elevated water concentrations during the direct DME synthesis process. (up to 12 mol %, see Figure 6b).

The dehydrogenation rates of methanol are significantly higher than those of methanol formation, so the reactor size is largely negligible compared to the latter. Consequently, although the number of reaction steps is reduced in the direct DME synthesis, both the

Reaction Chemistry & Engineering Accepted Manuscript

total reactor volume and catalyst mass of the direct route are much higher than the combined values of both reactors in the indirect route. Therefore, the main advantage of the direct route in relation to the indirect route is a higher CO_2 single-pass conversion, corresponding to a higher overall CO_2 conversion to DME (95.3% vs. 91.7%).

Table 5. Reactor configuration details of both synthesis routes.

Process	Configuration	Length (m)	Diameter (cm)	Number of tubes	Catalyst bed Volume (m^3)	Catalyst bed Mass (ton)	U ($W \cdot m^{-2} \cdot K^{-1}$)
Direct DME synthesis	Multitube reactor with cooling fluid	15	3.81	98,000*	1676.0	1879.6	300
Methanol synthesis	Multitube reactor with cooling fluid	15	3.81	49,000	838.0	1005.6	500
Methanol dehydration	Adiabatic reactor	10	125	1	12.5	11.0	-

*Two reactor modules with 49,000 each are considered in the cost estimation.

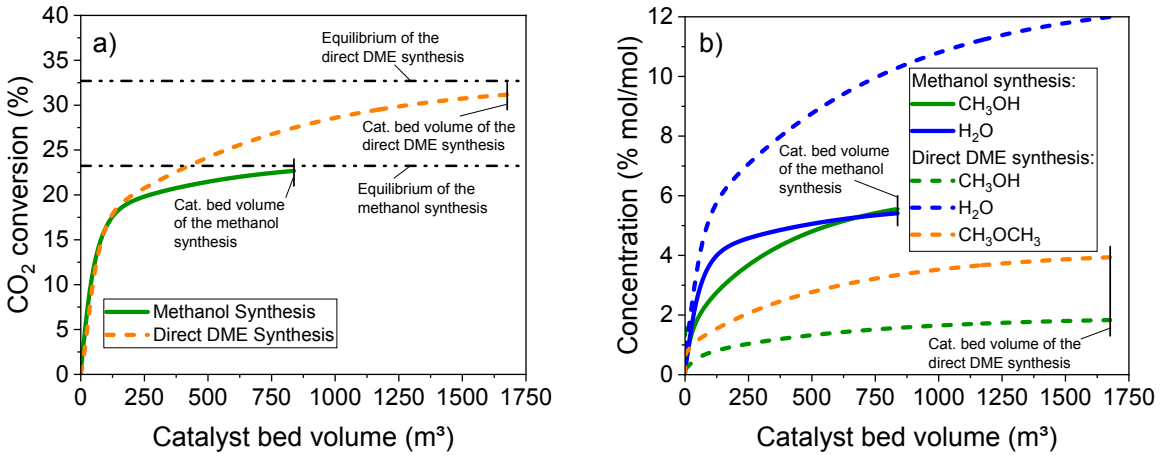


Figure 6. Simulated profiles along the catalyst bed. Total catalyst bed volume: 838 m^3 (methanol synthesis), 1676 m^3 (direct DME synthesis). a) CO_2 conversion. b) Concentration of MeOH, H_2O, and DME (% mol/mol).

4.3 Energy analysis

D'Ambrosio et al. (79) and Dieterich et al. (18) reported that external heat procurement is necessary in the direct DME synthesis even with heat integrated recovery. However, in the configurations proposed of the present work, both the direct and the indirect DME synthesis routes are self-sufficient in terms of heat. This contrast is probably because (i) in the previous studies purge stream combustion was not considered, although being a

Reaction Chemistry & Engineering Accepted Manuscript

valuable source of heat, and (ii) in our work an improved heat integration allows an improved management of heat streams. A further valorization of the purge streams might be to separate H_2 and CO_2 from inert gases (e.g., via membranes) and recycle the reactants, but this was beyond the scope of the present study.

In Table 6, the power requirements for both process routes are presented. The direct route has a slightly lower total power demand compared to the indirect route (93.4 vs. 98.5 MW), showing that the required power for the refrigeration cycle in the direct route was less than the extra compression power needed in the indirect route for feed and recycle compression, due to the latter lower single-pass conversion. However, the net power requirement of the direct route is higher (66.9 vs. 55.1 MW). This is caused by the lower power generation of the water Rankine cycle in the direct route, due to a lower purge stream than the indirect route (the purge stream combustion is a heat source for the water cycle), i.e., more reactant is being converted to DME instead of being combusted.

When expressed relative to DME, the net power requirements amount to 2.3 MJ/kg_{DME} for the direct route and 1.9 MJ/kg_{DME} for the indirect route. These values are relatively low (6.6 - 8%) compared to the lower heating value of DME (28.6 MJ/kg_{DME}), although not negligible.

While the pressure of H_2 feed was set to 1 bar, there are commercial plants of water electrolysis able to operate at higher pressures (e.g. alkaline membranes, polymer exchange membranes). If the water electrolysis would be performed at increased pressure (e.g., 30 bar), the net required power of both DME process routes could be considerably further reduced, and the indirect route would be operable nearly self-sufficient in terms of power: it only requires 1.1 MW or 0.036 MJ/kg_{DME}.

Table 6. Power requirements for each process route. Values in MW.

Section	Process route	
	Direct	Indirect
Feed H_2 compression	59.42	61.63
Feed CO_2 compression	19.23	19.94[a]
Recycle stream recompression	7.67	13.45[a]
Refrigeration cycle	7.09	–
Compression in the methanol dehydration section	–	3.46
Subtotal	**93.41**	**98.48**

Reaction Chemistry & Engineering Accepted Manuscript

Water Rankine Cycle	–26.53	–43.37
Net required power	**66.87**	**55.11**
Special case: feed H_2 is provided at 30 bar		
Power savings in feed H_2 compression work	–52.13[b]	–54.07[b]
Net required power in the special case	**14.74**	**1.04**

[a]One recycled stream at 1.013 bar is mixed with feed CO_2 and recompressed together. The compression work for feed CO_2 alone was calculated, and the difference was considered recycle stream recompression. [b]Comparing a four-stage H_2 compression from 1 to 50 bar with a one-stage H_2 compression from 30 to 50 bar.

4.4 Exergy analysis

The exergy destruction and efficiency for each operation in the direct and indirect routes is presented in Figure 7, while the detailed exergy flow for each process is shown in the Grassmann diagrams of Figures 8 and 9. In the Grassmann diagrams, the Heat exergy flows are in red, the exergy destruction of each operation is in orange, and work is represented in blue. Exergy associated with mass flows are described using the same name adopted in the Aspen Plus simulations. Detailed exergy balances are provided in Section S5 of the SI.

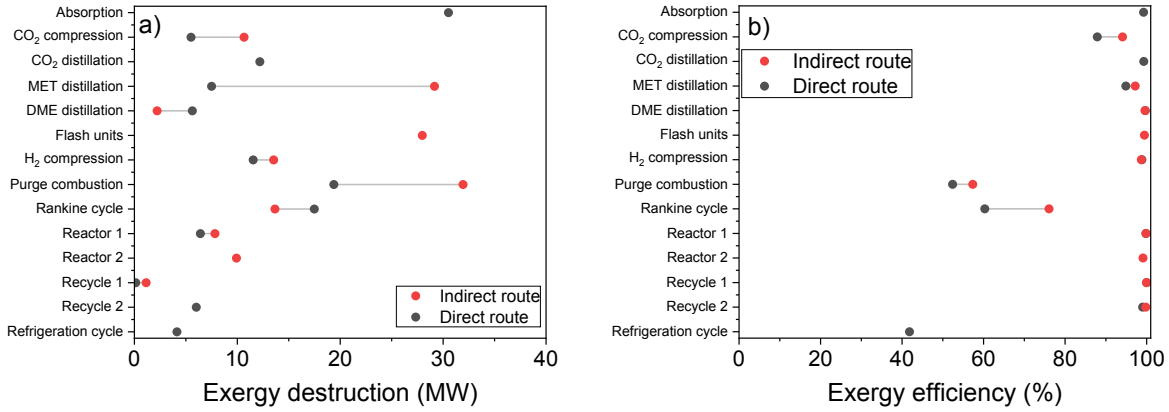


Figure 7. Exergy destruction in MW (a) and exergy efficiency in % (b) by operation. Absorption, CO_2 distillation, and Refrigeration cycle are only present in the direct route, while Flash units and Reactor 2 are only present in the indirect route.

In the direct route, although the absorption efficiency is considerably high (see Figure 7b), it represents the operation most responsible for exergy destruction (see Figure 7a). This

Reaction Chemistry & Engineering Accepted Manuscript

occurs because the inlet streams in the absorption operation are the reactor outlet stream (Stream 22) and the water-methanol absorbent stream (58-REC), which have high flow and therefore elevated exergy (see Figure 8). In addition to the absorption operation itself, it is necessary to cool Stream 22 to 303 K (to improve DME absorption), further destructing exergy.

The second operation that contributes most to exergy destruction in the direct route is the purge combustion (see Figure 7a). In this case, the exergy destruction is high due to the limited operation efficiency that is characteristic of processes involving combustion. The exergy of the flue gases leaving the plant is considered an exergy loss, since it is discarded directly into the environment (71-FLUE). It is however little compared to the exergy destruction of the Purge section (see Figure 8).

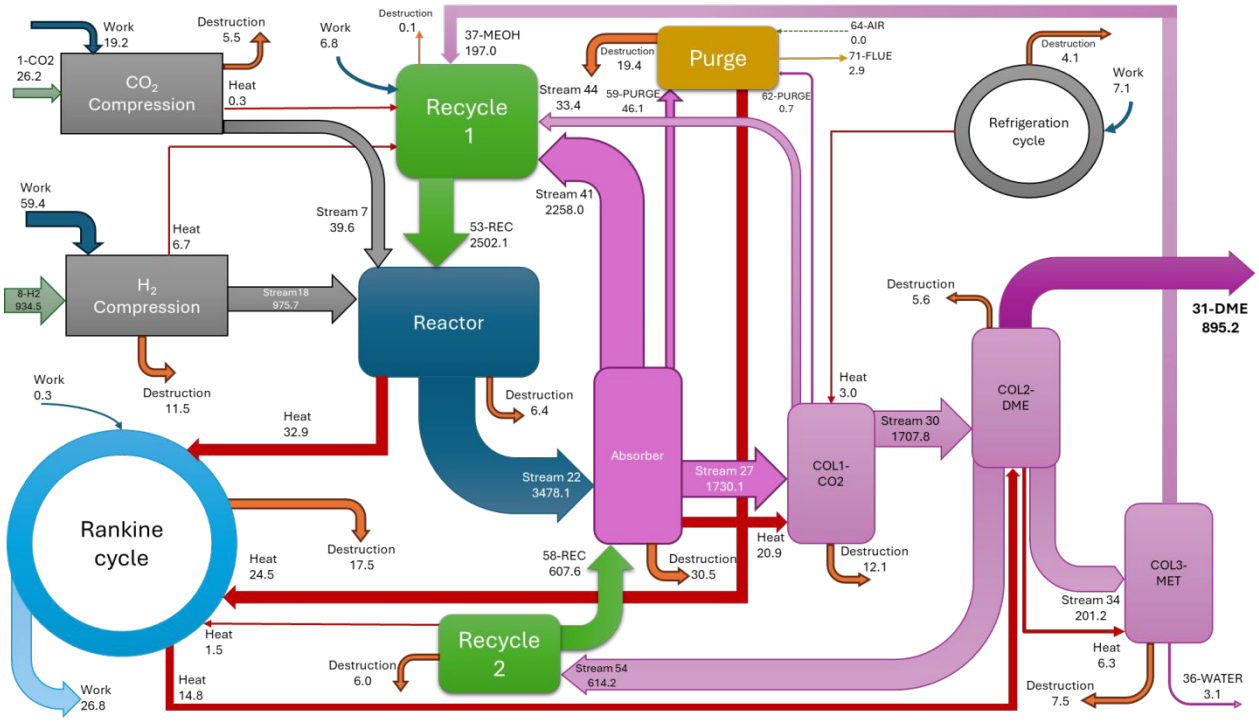


Figure 8. Direct DME synthesis, Grassmann Diagram of the direct DME synthesis. Values in MW.

Reaction Chemistry & Engineering Accepted Manuscript

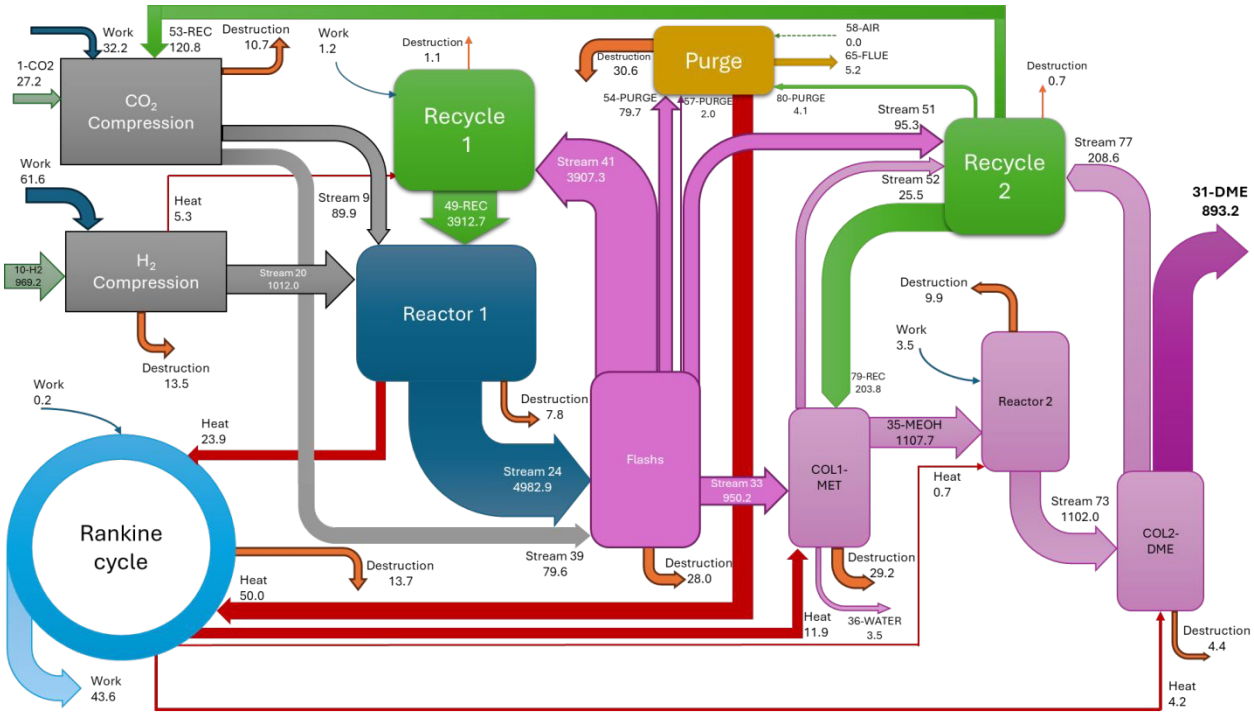


Figure 9. Indirect DME Synthesis, Grassmann Diagram. Values in MW.

The Rankine and refrigeration cycles are also characterized by efficiencies lower than the typically high efficiencies of the other operations in the direct route (see Figure 7b). The main point about these thermodynamic cycles is that they are limited by (i) the Carnot's efficiency and by (ii) restrictions imposed by real operation (e.g., compressors must receive pure vapor streams to protect the equipment from damages). Furthermore, the Rankine cycle is already an effort of heat recovery and redistribution as well as power generation.

Regarding the refrigeration cycle, a remarkable observation is: while heat flows from the CO_2 distillation column (COL1-CO2) to the refrigeration cycle, exergy flows in the reverse direction (see Figure 8). This phenomenon occurs because the heat transfer is observed at a temperature lower than 298.15 K (the reference temperature), and exergy is defined as the withdrawal from the reference state.

In the indirect route, there are three operations that mostly cause exergy destruction: purge, flashes 1 and 2 and methanol distillation (see Figure 7a). As previously mentioned, purge exergy destruction is related to the combustion in the furnace, which has normally limited exergy efficiency. The flash operations and methanol distillation in the indirect synthesis have high exergy efficiency (see Figure 7b), but, similarly to the adsorption

Reaction Chemistry & Engineering Accepted Manuscript

process in the direct route, they exhibit high exergy destruction. The exergy destruction in the flash operation control volume is more strongly associated with the cooling of the reactor outlet stream in Heat Exchanger 10 (H10) than with the flash process itself. Exergy destruction in the methanol distillation column can be attributed mainly to the heat transfer processes occurring in the reboiler and the condenser.

In the indirect route, most operations have high efficiency values, such as the DME distillation column, the first reactor and the recycles. The main difference is in the Rankine cycle, which is considerably more efficient in the indirect route (see Figure 7b). However, some operations in the indirect route are responsible for more exergy destruction even being more efficient, such as the methanol distillation and the purge (see Figure 7). This occurs because the mentioned operations require more exergy input in the indirect than in the direct route (see Figures 8 and 9).

Global exergy balances are provided in Table 7. Although the indirect route requires less work compared to the direct route, the former requires more H_2 and CO_2, as higher purge losses occur due to the lower reactant single-pass conversion. Overall, this trade-off is favorable for the direct route, which has a higher global exergy efficiency compared to the indirect route (87.1% vs. 84.9%). In the special case where H_2 is provided at 30 bar, the exergy efficiency of both routes increase considerably, and the direct route performance remains better than the one of the indirect route (91.8% vs. 89.5%).

The exergy efficiency values in this work are significantly higher than reported in our previous work on the methanol synthesis (76 - 78%) (16):

- First, the chemical exergy calculation applied here was updated compared to our previous work, as the dead state of the gas phase was considered to be atmospheric air (see Section 3.4). Consequently, the CO_2 feed stream, which is highly pure, does have a positive exergy even if it is under the reference temperature and pressure. This approach is more realistic than the commonly applied high heating value (HHV), as the effort to concentrate CO_2 from air (typically at 400 ppm) to 90 - 95% capturing rate, regarding optimal balance with heat utilization, in a carbon capture unit (CCU) is significant.
- Second, the design of the Rankine water cycle was significantly improved compared to our previous work, maximizing power generation given the conditions of each process.

Reaction Chemistry & Engineering Accepted Manuscript

Table 7. Global exergy balance of both process routes. Values in MW.

	Direct route	Indirect route
Inlet		
H_2	934.47	969.25
CO_2	26.22	27.20
Work	66.87	55.11
Total	**1027.56**	**1051.56**
Outlet		
DME	895.18	893.17
Exergy Loss	5.97	8.80
Exergy Destruction	126.41	149.59
Total	**1027.56**	**1051.56**
Exergy Efficiency	**87.1 %**	**84.9 %**

4.5 Techno-economic analysis

Figure 10 presents the equipment costs for the direct (D) and the indirect (I) routes. A comprehensive table of individual equipment costs, accompanied by the essential key factors, is available in Section S6 of the SI. The equipment costs are classified into sub-processes, in which main equipment (e.g. reactor) are grouped together with auxiliary equipment (e.g. heat exchanger), similarly to the exergy analysis. A detailed group assignment is provided in Section S6 of the SI.

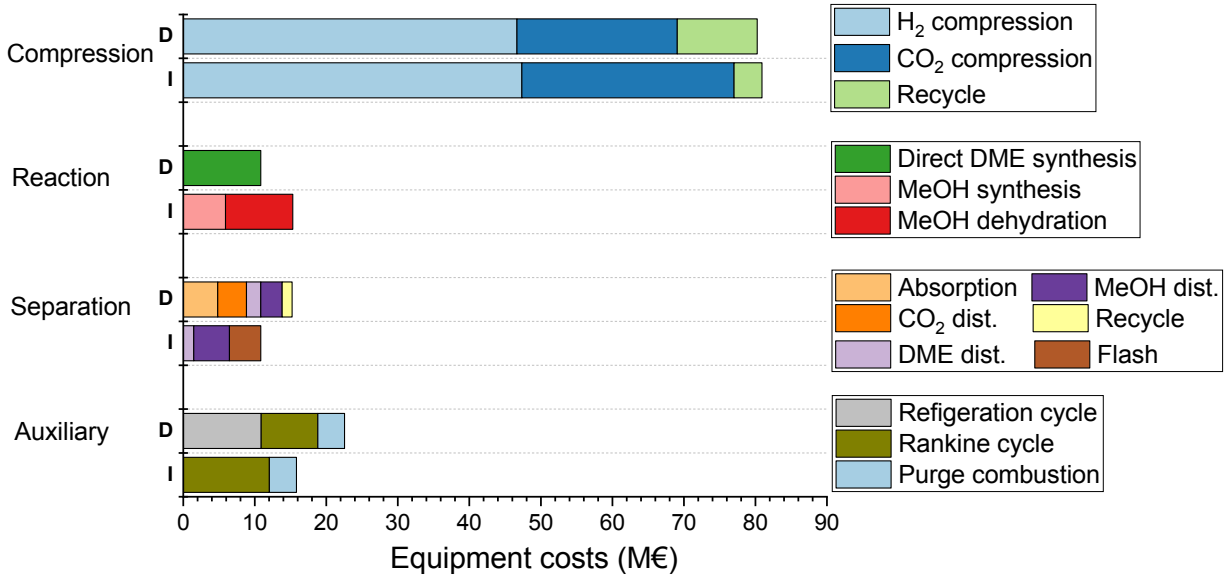


Figure 10. Distribution of equipment costs for the direct (D) and the indirect (I) process routes, classified into subprocesses.

Reaction Chemistry & Engineering Accepted Manuscript

In the compression section, the equipment costs of the direct and indirect route are similar (0.67 M€ or 0.83% higher for the indirect route). On one hand, the direct route achieves a higher single-pass conversion, resulting in lower feed and recycle flow rates, and consequently, smaller compressor units are needed. On the other hand, the direct route consists of a more complex process configuration, and particularly the CO_2 recycle contributes significantly to the compressor costs. In the indirect route, Stream 52, a recycle stream rich in CO_2, is mixed with the fresh CO_2 feed stream before compression. As a result, equipment costs attributed to feed CO_2 compression also include the compression requirements of this recycle stream. This explains why the indirect route appears to have substantially higher CO_2 feed compression costs and significantly lower recycle compression costs.

In the reaction section, the indirect route is significantly more expensive (4.47 M€ or 41%). This discrepancy is not attributable to the reactor units, as their size and cost are higher in the direct route (see Table 5). Instead, the higher costs of the indirect route are associated with the heat integration strategy implemented in the methanol dehydration section, which requires several heat exchangers and an additional compressor.

In the separation section, the direct route is considerably more expensive than the indirect route (2.48 M€ or 23%). This difference is a result of the fact that separating the more complex mixture of substances is a more cost intense in the direct route, additionally requiring a distillation column for CO_2 separation and an absorber. In the indirect route, the flash subprocess appears to contribute substantially to the total separation costs. However, this is not due to the flash units themselves, which are generally inexpensive, but rather to the heat exchangers associated to this subprocess.

In the auxiliary section, the direct route is significantly more expensive than the indirect route (6.73 M€ or 42.5%). On the one hand, the higher overall reactant conversion achieved in the direct route results in lower purge flow rates, reducing the size and cost of the purge combustion system and the water Rankine cycle. Consequently, these subprocesses are less expensive in the direct synthesis route. On the other hand, only the direct route requires a refrigeration cycle to support the cryogenic distillation process, which represents a substantial additional cost.

Reaction Chemistry & Engineering Accepted Manuscript

Overall, the equipment costs of the direct route are 126.94 M€, which are moderately higher (4.06 M€ or 3.3%) compared to the indirect route (122.88 M€). In terms of total capital investment (TCI), the direct route costs 710.86 M€, while the indirect route costs 688.12 M€.

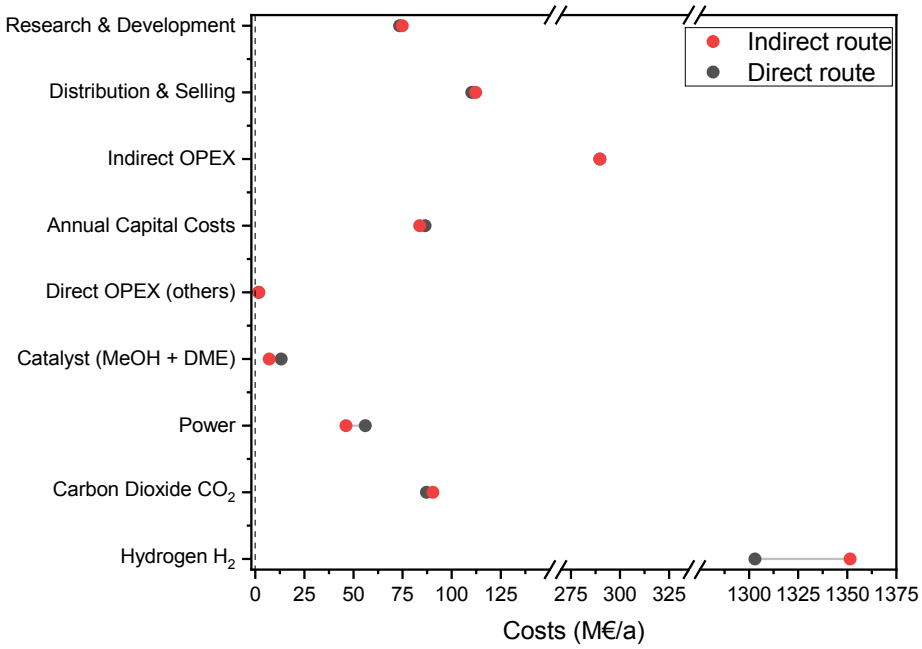


Figure 11. Distribution of total costs (ACC and OPEX) for the direct (D) and the indirect (I) route.

The total costs, including direct and indirect OPEX, annual capital costs, distribution and selling as well as research and development costs are represented in Figure 11. Further details of indirect and direct OPEX calculations can be found in Section S6 of the SI.
The direct route has lower costs for hydrogen (48.49 M€/a or 3.7% lower) and for carbon dioxide (3.24 M€/a or 3.7% lower), due to the more efficient global conversion compared to the indirect route. However, the direct route has higher annual capital costs (2.77 M€/a or 3.3% higher), as previously discussed, higher catalyst costs (6.06 M€/a or 85.3% higher), due to the much larger total reactor volume (1676 vs 850.5 m³, see Section 4.2), and higher power costs (9.85 M€/a or 21.3% higher), due to a higher net power consumption (21 % higher, see Section 4.3). Overall, this compromise is advantageous for the direct route, which has total annual net production costs (NPC) of 1,837.20 M€/a, which is 33.12 M€/a or 1.8 % less compared to the indirect route (1,870.32 M€). If these

Reaction Chemistry & Engineering Accepted Manuscript

costs are allocated to the simulated production capacity (approx. 836.8 kt/a), the net production costs amount to 2195.4 €/t_{DME} for direct DME synthesis and 2234.9 €/t_{DME} for indirect DME synthesis.

The relative difference of 1.8% might seem of low significance, especially due to the uncertainties involved in a techno-economic analysis. However, this relative difference is offset by the high flow rate and high price of H_2. In addition, the conversion (or processing) costs were calculated. The conversion costs are defined as the expenses related to the transformation of the feedstock into the targeted product. The costs of the minimum (or stoichiometric) amount of hydrogen and carbon dioxide required to produce DME, i.e. 6 mol of H_2 and 2 mol of CO_2 per mol of DME, or 0.2626 ton of H_2 and 1.9106 ton of CO_2 per ton of DME were calculated. Then, these minimum costs were subtracted from the NPC. Only the costs of H_2 and CO_2 which exceed this minimum amount are accounted for in the conversion costs (i.e., the H_2 and CO_2 that are lost in the purge streams).

The conversion costs are 704.42 €/t_{DME} for the direct route and 743.97 €/t_{DME} for the indirect route. That is a significant 5.6% increase in conversion costs for the indirect route compared to the direct synthesis route.

Several uncertainties inherently affect economic evaluations, including capital cost scaling errors, volatile market prices for raw materials and utilities, and thermodynamic assumptions inherent to process flowsheet simulations. Nevertheless, because both routes were evaluated using a consistent methodology and unified baseline assumptions, the relative economic comparison remains robust and meaningful, even if absolute cost estimates differ from actual market values.

A sensitivity analysis was conducted in the following section to demonstrate the impact of the costs of the reactants (hydrogen, carbon dioxide) and of the power on the net production costs of DME. Results are presented in Figure 12.

Reaction Chemistry & Engineering Accepted Manuscript

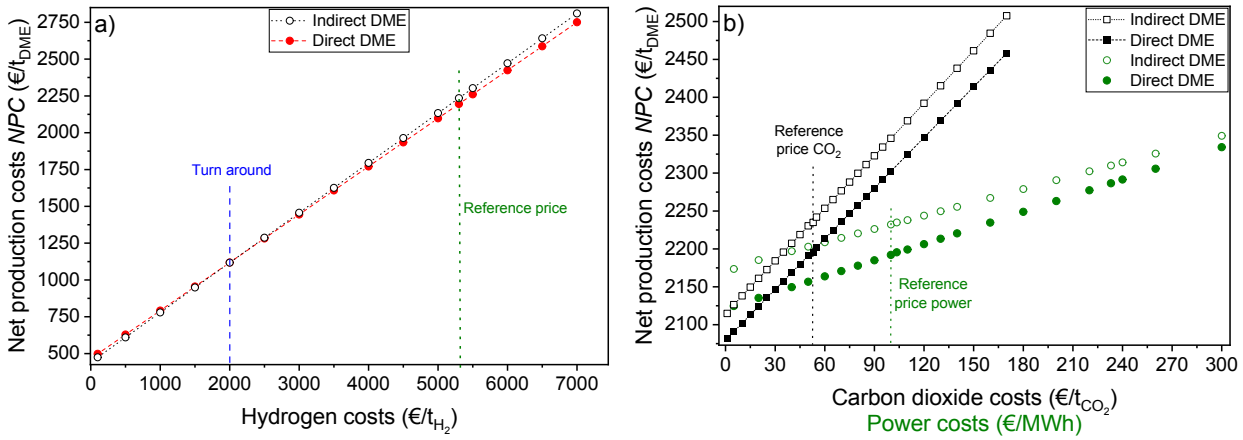


Figure 12. Sensitivity analysis of hydrogen (a), carbon dioxide and power (b) costs for the direct and the indirect routes.

For the direct DME route a total of 70.9% of the NPC is attributed to hydrogen costs, while carbon dioxide costs account for 4.8% and power costs 3.1%. In direct comparison, the breakdown for the indirect synthesis route exhibits a slight discrepancy, with hydrogen costs accounting for 72.3% of the NPC. The cost of carbon dioxide accounts for 4.8%, while the cost of power accounts for 2.5% of the NPC indicating that the fluctuations in the costs of carbon dioxide and electricity have a limited effect on the net production costs of DME, as illustrated in Figure 12b. Most importantly, as illustrated in Figure 12a the NPC curves of the two processes intersect when the hydrogen price is around 2046 €/t_{H2}, corresponding to an NPC of 1133.3 €/t_{DME}. According to this analysis, the direct route is more economical if the hydrogen price exceeds 2046 €/t_{H2}, and the indirect synthesis becomes more economical if the hydrogen price sinks below this value. As the current price of green H_2 is more than 2.5 times higher than this threshold (5300 €/t_{H2} considered in the present work), the direct route is more economical even in a scenario of 60% price drop, although the difference diminishes progressively with a reduction of the hydrogen price.

A review of the estimated average price of hydrogen from fossile feedstocks (2670 €/t_{H2}) (73) produced via Steam Methane Reforming (SMR) in the European Union in 2021 reveals that this price exceeds the previously stated break-even price (indirect vs. direct DME synthesis) of 2046 €/t_{H2}.

Reaction Chemistry & Engineering Accepted Manuscript

On this basis, the net production costs of direct DME synthesis - even when using gray hydrogen - would have been lower than those of indirect DME synthesis.

As illustrated in Figure 12b, the net production costs are sensitive to the CO_2 price and energy costs. The direct route has the lowest NPC regardless of the CO_2 price, even for 0 €/t_{CO2}.

A detailed analysis of electricity prices reveals that direct DME synthesis is more cost-effective than indirect DME synthesis within the range of 0 - 300 €/MWh. Should power costs continue to rise, the two curves should intersect at a very high electricity price of 420.8 €/MWh (NPC = 2419.95 €/t_{DME}), point at which the indirect DME synthesis becomes more cost-effective than the direct DME synthesis route. However, it is unlikely that the power price would vary significantly without affecting the price of green hydrogen as well, as sustainable electricity accounts for the majority of the costs of green hydrogen.

A second sensitivity analysis was performed, this time varying the initial pressure of feed hydrogen. This analysis was restricted to the direct route. As mentioned in Section 4.3, while a pressure of 1 bar was considered up to this point as reference, water electrolysis can be operated at higher pressures such as 30 bar (e.g. alkaline water electrolysis, anion exchange membrane water electrolysis, and polymer exchange membrane water electrolysis). Although high-pressure electrolysis is more expensive and slightly less efficient due to an increased reversible voltage, it is generally advantageous because of the opportunity to reduce capital and operating costs associated with hydrogen compression afterwards, as shown in Section 4.3.

Since a detailed analysis of the effects of operating pressure in the water electrolysis is out of the scope of this work, this sensitivity analysis focused on the effect of feed H_2 pressure on the compressor and power costs of the DME synthesis, considering a constant H_2 price.

Reaction Chemistry & Engineering Accepted Manuscript

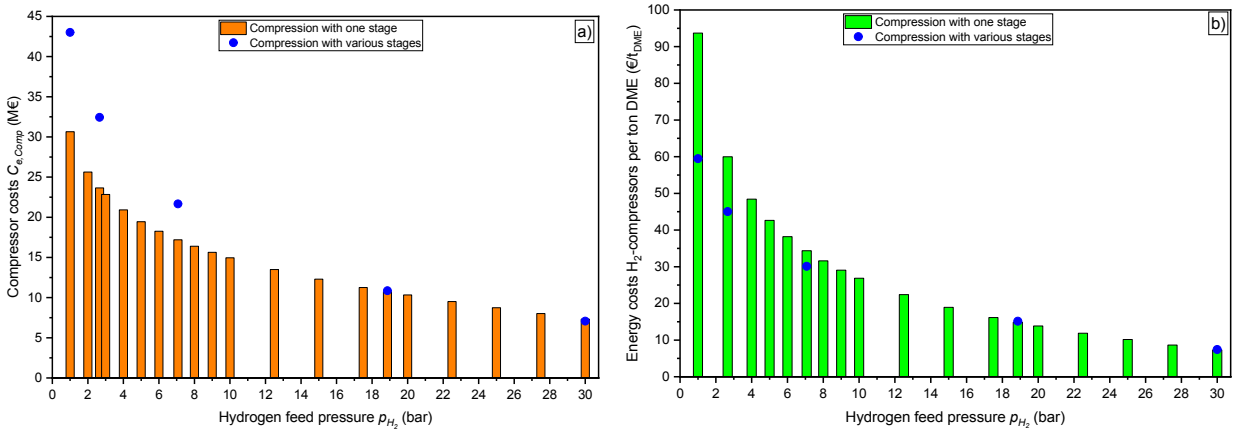


Figure 13. Cost trends for hydrogen compressor equipment (a) and the associated energy costs for hydrogen compression (b). The bars represent a single compression stage, and the points represent a multi-stage compression system, as used in the TEA, depending on the feed pressure.

The analysis was performed for both a single stage compression (see bars in Figure 13) and a multistage compressor (see dots in Figure 13 for selected pressures). For the multistage compressor, the following feed pressures and number of stages were selected: 1.01 bar (4 stages), 2.66 bar (3 stages), 7.07 bar (2 stages), 18.8 bar (2 stages), and 30 bar (1 stage). It was assumed that the equipment costs for the heat exchangers of the multistage compressor will remain constant, as these are also utilized at other points in the process to recover heat. It was also assumed that heat could be recovered from elsewhere in the plant, maintaining the status of self-sufficiency in heat, as there are several streams in the flowsheet with potential to provide heat at adequate temperatures. Results are shown in in Figure 13. By operating the electrolyzers at 30 bar, the equipment costs for the hydrogen compressors in the DME synthesis can be considerably reduced, from approximately 43.02 M€ to 7.39 M€ (-82.8%), as well as the associated power costs, from 59.47 €/t_{DME} to 7.41 €/t_{DME} (-87.4%). This results in a decrease in the NPC from 2195 €/t_{DME} to 2067 €/t_{DME} (-5.8%), and a significant improvement in the conversion costs: from 704.4 €/t_{DME} to 576.0 €/t_{DME} (-18.2%).

5. Summary and Conclusions

Reaction Chemistry & Engineering Accepted Manuscript

This work compared the direct and indirect routes to DME from renewable H_2 and captured CO_2 on a common basis using the same feedstock specification and plant capacity (836.8 kt a^{-1}), a similar heat-integration strategy, and the same cost basis.

A kinetic model for the direct DME synthesis over Cu/ZnO/ZrO_2 + H-FER-20 was reparametrized based on 1320 experimental points collected over 1200 h time on stream, and extended to utilization of pure H_2/CO_2 Our model predicts DME and methanol molar fractions with mean relative errors of 8% and 11%, with no significant difference between training and validation sets. A further advantage for the present comparison is that the kinetic models used for the direct DME synthesis and the methanol synthesis of the indirect route were fitted to experiments performed with the same methanol catalyst (Cu/ZnO/ZrO_2). Differences between the routes therefore reflect the process configurations themselves rather than differences in catalyst formulation or in the experimental basis from which the kinetics were derived. This addresses one of the limitations of earlier techno-economic comparisons, which relied on kinetic models fitted to short experiments with pronounced deactivation, or to a single feed composition, and which did not always draw the two reaction models from a common catalytic data basis with the same methanol catalyst (Cu/ZnO/ZrO_2).

With a water Rankine cycle recovering the reaction enthalpy and a fired heater burning the purge gas, both routes are fully self-sufficient in heat, in contrast to earlier studies, which reported a residual external heat demand for both. Within the configurations proposed here, heat is therefore not a differentiator between the routes, but electricity demand and capital costs are.

The direct route converts more CO_2 to DME (95.3% vs 91.7% overall), which cuts purge losses and therefore feedstock consumption. This comes at a cost on three fronts. (i) The direct DME synthesis reactor is twice the size of the methanol reactor (indirect route), since the high-water content that builds up along the bed suppresses the reaction rates: beyond 17% CO_2 conversion the kinetics slow markedly, and the last 15 percentage points of conversion require a catalyst bed twelve times larger than the fast-kinetics region. (ii) The separation train is more demanding, requiring an absorption column and a cryogenic

Reaction Chemistry & Engineering Accepted Manuscript

CO_2/DME distillation with a dedicated two-stage refrigeration cycle. (iii) The net power demand is 21% higher. Exergetically the balance still favors the direct route (87.1% vs 84.9%), as the hydrogen saved is worth more than the additional work consumed.

Economically, the direct route is slightly less expensive (2195.4 vs 2234.9 €/t_{DME}). Because hydrogen accounts for 70.9% for direct DME route and 72.3% for indirect DME route of the net production costs, this 1.8% margin understates the difference between the processes. On a conversion-cost basis (i.e., NPC minus the stoichiometric H_2 and CO_2), the direct route is 5.6% cheaper (704.42 vs 743.97 €/t_{DME}). Both, CO_2 and electricity prices have little influence: the direct route remains advantageous for any CO_2 price and for an electricity price up to 420.8 €/MWh. The hydrogen price is the decisive variable, with a crossover at 2046 €/t_{H2}, which is below any current or near-term green hydrogen price, so the direct route remains preferable even under a 60% price drop. At gray-hydrogen prices from SMR processes (2021: 2670 €/t_{H2}), by contrast, the direct route becomes also cheaper.

Finally, feeding hydrogen at 30 bar from pressurized electrolysis reduces the direct-route compressor cost by 83%, the net power consumption by 87%, and the net production costs by 5.8% (to 2067 €/t_{DME}), while the conversion costs decrease by 18% (704.4 €/t_{DME} to 576.0 €/t_{DME}).

Two extensions to this comparison appear particularly worthwhile. First, by including hydrogen production in the techno-economic analysis rather than upstreaming it, the optimal electrolyzer pressure can be assessed, as the compression savings reported above and the electrolyzer penalty (more expensive and less efficient) move in opposite directions. Second, intermediate condensation of methanol and water has been reported to improve both the methanol synthesis and the direct DME synthesis (16, 80), relieving equilibrium and water-inhibition limitations that constrain per-pass conversion. Introducing intermediate condensation into both flowsheets could change the ranking reported here, and a comparison on that basis would be a natural next step.

Conflict of Interests

Reaction Chemistry & Engineering Accepted Manuscript

There is no conflict of interests to declare.

Acknowledgements

The authors acknowledge the funding of the Materials and Technologies for the Energy Transition (MTET) program from the Helmholz Association. We gratefully acknowledge the contributions of Sebastian Grewe and Ricki Drexler for their valuable assistance in conducting the experiments and rebuilding the experimental setup.

References

1. Core Writing Team HLaJRe. Climate Change 2023: Synthesis Report. Contribution of Working Groups I, II and III to the Sixth Assessment Report of the Intergovernmental Panel on Climate Change. IPCC, Geneva, Switzerland,; 2023.
2. Duyck S. The Paris Climate Agreement and the Protection of Human Rights in a Changing Climate. Yearbook of International Environmental Law. 2017;26:3-45.
3. Geissdoerfer M, Savaget P, Bocken NMP, Hultink EJ. The Circular Economy – A new sustainability paradigm? Journal of Cleaner Production. 2017;143:757-68.
4. Oliver D. Doleski TK, Michael Metzger, Stefan Niessen, Sebastian Thiem. Digitale Dekarbonisierung - Technologieoffen die Klimaziele erreichen2021.
5. Azizi Z, Rezaeimanesh M, Tohidian T, Rahimpour MR. Dimethyl ether: A review of technologies and production challenges. Chem Eng Process. 2014;82:150-72.
6. Delgado Otalvaro N, Sogne G, Herrera Delgado K, Wild S, Pitter S, Sauer J. Kinetics of the direct DME synthesis from CO(2) rich syngas under variation of the CZA-to-gamma-Al(2)O(3) ratio of a mixed catalyst bed. RSC Adv. 2021;11(40):24556-69.
7. Fleisch TH, Basu A, Sills RA. Introduction and advancement of a new clean global fuel: The status of DME developments in China and beyond. Journal of Natural Gas Science and Engineering. 2012;9:94-107.
8. Ortega C, Kolb G. DME-to-Hydrocarbon over an MFI Zeolite: Product Selectivity Controlled by Oxygenates under the Kinetic Regime. Ind Eng Chem Res. 2019;58(51):22893-904.
9. Yeoman AM, Lewis AC. Global emissions of VOCs from compressed aerosol products. Elementa: Science of the Anthropocene. 2021;9(1).
10. Müller M, Hübsch U. Dimethyl Ether. Ullmann's Encyclopedia of Industrial Chemistry2000.
11. Semelsberger TA, Borup RL, Greene HL. Dimethyl ether (DME) as an alternative fuel. J Power Sources. 2006;156(2):497-511.
12. Zimmermann M, Otto TN, Powietzka B, Neumann-Walter D. Umsetzung von Dimethylether zu Kraftstoffen mit hierachischen Zeolithkatalysatoren. Chemie Ingenieur Technik. 2015;87(12):1748-59.
13. Chmielarz L. Dehydration of Methanol to Dimethyl Ether—Current State and Perspectives. Catalysts. 2024;14(308).
14. Ott J, Gronemann V, Pontzen F, Fiedler E, Grossmann G, Kersebohm DB, et al. Methanol: John Wiley & Sons Ltd; 2012.
15. Freepik. Flaticon Icons [Available from: https://www.flaticon.com/authors/freepik.

Reaction Chemistry & Engineering Accepted Manuscript

16. Lacerda de Oliveira Campos B, John K, Beeskow P, Herrera Delgado K, Pitter S, Dahmen N, et al. A Detailed Process and Techno-Economic Analysis of Methanol Synthesis from H2 and CO2 with Intermediate Condensation Steps. Processes. 2022;10(8).
17. Ateka A, Ereña J, Bilbao J, Aguayo AT. Kinetic modeling of the direct synthesis of dimethyl ether over a CuO-ZnO-MnO/SAPO-18 catalyst and assessment of the CO2 conversion. Fuel Process Technol. 2018;181:233-43.
18. Dieterich V, Neumann K, Niederdränk A, Spliethoff H, Fendt S. Techno-economic assessment of renewable dimethyl ether production pathways from hydrogen and carbon dioxide in the context of power-to-X. Energy. 2024;301.
19. Kartohardjono S, Adji BS, Muharam Y. CO2 Utilization Process Simulation for Enhancing Production of Dimethyl Ether (DME). International Journal of Chemical Engineering. 2020;2020:1-11.
20. Rafiee A. Staging of di-methyl-ether (DME) synthesis reactor from synthesis gas (syngas): Direct versus indirect route. Chemical Engineering Research and Design. 2020;163:157-68.
21. Wenwu X, Meiqin W, Shihe C, Huairong Z, Yinglong W, Zhaoyou Z, et al. Sustainable dimethyl ether synthesis pathway based on MSW gasification and carbon dioxide utilization. Energy. 2025;337:138561.
22. Wu T-W, Chien IL. A novel energy-efficient process of converting CO2 to dimethyl ether with techno-economic and environmental evaluation. Chemical Engineering Research and Design. 2022;177:1-12.
23. Banivaheb S, Pitter S, Delgado KH, Rubin M, Sauer J, Dittmeyer R. Recent Progress in Direct DME Synthesis and Potential of Bifunctional Catalysts Chemie Ingenieur Technik. 2022;94(3):240-55.
24. Dahmen N, Arnold U, Djordjevic N, Henrich T, Kolb T, Leibold H, et al. High pressure in synthetic fuels production. The Journal of Supercritical Fluids. 2015;96:124-32.
25. Dieterich V. Power-to-liquid via synthesis of methanol, DME or Fischer–Tropsch-fuels: a review. 2020.
26. Mevawala C, Jiang Y, Bhattacharyya D. Techno-economic optimization of shale gas to dimethyl ether production processes via direct and indirect synthesis routes. Appl Energ. 2019;238:119-34.
27. Andrea B, Yuchu C, David C, Benoît C. Direct DME Synthesis from Syngas: a Technoeconomic Model-based Investigation. In: Sauro P, Flavio M, Giulia Luisa B, Davide M, editors. 30th European Symposium on Computer Aided Process Engineering. 48: Elsevier; 2020. p. 655-60.
28. Nakyai T, Saebea D. Exergoeconomic comparison of syngas production from biomass, coal, and natural gas for dimethyl ether synthesis in single-step and two-step processes. Journal of Cleaner Production. 2019;241.
29. An X, Zuo Y-Z, Zhang Q, Wang D-z, Wang J-F. Dimethyl Ether Synthesis from CO2 Hydrogenation on a CuO−ZnO−Al2O3−ZrO2/HZSM-5 Bifunctional Catalyst. Ind Eng Chem Res. 2008;47(17):6547-54.
30. Graaf GH, Scholtens H, Stamhuis EJ, Beenackers AACM. Intra-particle diffusion limitations in low-pressure methanol synthesis. Chem Eng Sci. 1990;45(4):773-83.
31. Graaf GH, Stamhuis EJ, Beenackers AACM. Kinetics of low-pressure methanol synthesis. Chem Eng Sci. 1988;43(12):3185-95.

Reaction Chemistry & Engineering Accepted Manuscript

32. Rodrigues Niquini G, Lacerda de Oliveira Campos B, Herrera Delgado K, Pitter S, Sauer J. Experimental study and comprehensive kinetic modeling of the direct dimethyl ether synthesis on Cu/ZnO/ZrO2 and H-FER-20. Chem Eng J. 2024;480:147968.
33. Polierer S, Guse D, Wild S, Herrera Delgado K, Otto TN, Zevaco TA, et al. Enhanced Direct Dimethyl Ether Synthesis from CO2-Rich Syngas with Cu/ZnO/ZrO2 Catalysts Prepared by Continuous Co-Precipitation. Catalysts. 2020;10(8):816.
34. Guse D, Polierer S, Wild S, Pitter S, Kind M. Improved Preparation of Cu/Zn-Based Catalysts by Well-Defined Conditions of Co-Precipitation and Aging. Chemie Ingenieur Technik. 2022;94(3):314-27.
35. Guse D, Warmuth L, Herfet M, Adolf K, Zevaco TA, Pitter S, et al. Seeding as a Decisive Tool for Increasing Space-Time-Yields in the Preparation of High-Quality Cu/ZnO/ZrO2 Catalysts. Catalysts. 2024;14(8):517.
36. Lacerda de Oliveira Campos B, Herrera Delgado K, Wild S, Studt F, Pitter S, Sauer J. Surface reaction kinetics of the methanol synthesis and the water gas shift reaction on Cu/ZnO/Al2O3. Reaction Chemistry & Engineering. 2021;6(5):868-87.
37. Wild S, Lacerda de Oliveira Campos B, Zevaco TA, Guse D, Kind M, Pitter S, et al. Experimental investigations and model-based optimization of CZZ/H-FER 20 bed compositions for the direct synthesis of DME from CO2-rich syngas. Reaction Chemistry & Engineering. 2022;7(4):943-56.
38. Peláez R, Marín P, Ordóñez S. Direct synthesis of dimethyl ether from syngas over mechanical mixtures of CuO/ZnO/Al2O3 and γ-Al2O3: Process optimization and kinetic modelling. Fuel Process Technol. 2017;168:40-9.
39. Lacerda de Oliveira Campos B, Herrera Delgado K, Pitter S, Sauer J. Development of Consistent Kinetic Models Derived from a Microkinetic Model of the Methanol Synthesis. Ind Eng Chem Res. 2021;60(42):15074-86.
40. Slotboom Y, Bos MJ, Pieper J, Vrieswijk V, Likozar B, Kersten SRA, et al. Critical assessment of steady-state kinetic models for the synthesis of methanol over an industrial Cu/ZnO/Al2O3 catalyst. Chem Eng J. 2020;389.
41. Seidel C, Jörke A, Vollbrecht B, Seidel-Morgenstern A, Kienle A. Kinetic modeling of methanol synthesis from renewable resources. Chem Eng Sci. 2018;175:130-8.
42. Rodrigues Niquini G, Herrera Delgado K, Pitter S, Sauer J. Kinetics of CO2 hydrogenation to methanol on Cu/ZnO/ZrO2 based on an extensive dataset Reaction Chemistry & Engineering. 2026.
43. Bercic G, Levec J. Catalytic dehydration of methanol to dimethyl ether. Kinetic investigation and reactor simulation. Ind Eng Chem Res. 1993;32(11):2478-84.
44. Energy S. The Haru Oni Hydrogen Plant [Available from: https://www.siemens-energy.com/global/en/news/magazine/2021/haru-oni.html.
45. Peletiri SP, Rahmanian N, Mujtaba IM. CO2 Pipeline Design: A Review. Energies. 2018;11(9).
46. Porter RTJ, Fairweather M, Pourkashanian M, Woolley RM. The range and level of impurities in CO2 streams from different carbon capture sources. International Journal of Greenhouse Gas Control. 2015;36:161-74.
47. Guo Y, Li G, Zhou J, Liu Y. Comparison between hydrogen production by alkaline water electrolysis and hydrogen production by PEM electrolysis. IOP Conference Series: Earth and Environmental Science. 2019;371(4):042022.
48. Porter RTJ, Fairweather M, Kolster C, Mac Dowell N, Shah N, Woolley RM. Cost and performance of some carbon capture technology options for producing different

Reaction Chemistry & Engineering Accepted Manuscript

quality CO 2 product streams. International Journal of Greenhouse Gas Control. 2017;57:185-95.
49. Moran MJHNSDDBaMBB. Fundamentals of Engineering Thermodynamics. 8th ed: John Wiley & Sons; 2014.
50. VDI Heat Atlas. 2 ed: Springer Berlin, Heidelberg; 2010. XLII, 1584 p.
51. Gruber M. Detaillierte Untersuchung des Wärme- und Stofftransports in einem Festbett-Methanisierungsreaktor für Power-to-Gas Anwendungen: Karlsruher Institut für Technologie (KIT); 2020.
52. Clariant. MegaMax 800 – High-performance catalyst for methanol synthesis: Clariant; 2017 [Available from: https://www.clariant.com/en/Solutions/Products/2019/02/14/13/39/MegaMax-800.
53. Bercic G, Levec J. Catalytic dehydration of methanol to dimethyl ether. Kinetic investigation and reactor simulation. Industrial \& Engineering Chemistry Research. 1993;32(11):2478-84.
54. Institute AP. Burners for Fired Heaters in General Refinery Services. In: Institute AP, editor. 3rd ed. ed. Washington, DC, USA2014.
55. Cordero-Lanzac T, Ramirez A, Navajas A, Gevers L, Brunialti S, Gandía LM, et al. A techno-economic and life cycle assessment for the production of green methanol from CO2: catalyst and process bottlenecks. Journal of Energy Chemistry. 2022;68:255-66.
56. Fraga MMC, Campos BLdO, Lisboa MS, Almeida TBd, Costa AOSd, Lins VdFC. Analysis of a Brazilian Thermal Plant Operation Applying Energetic and Exergetic Balances. Brazilian Journal of Chemical Engineering. 2018;35(4):1395-403.
57. Towler G, Sinnott R. Chemical Engineering Design - Principles, Practice and Economics of Plant and Process Design. 3. ed: Katey Birtcher; 2022.
58. Green DWS, M.Z. Perry's Chemical Engineers' Handbook. 9th ed: McGraw Hill 2018.
59. Roy N, Maik B, Arne G. Techno-economic assessment of a wood-based biorefinery concept for the production of polymer-grade ethylene, organosolv lignin and fuel. Bioresource Technology. 2016;200:928-39.
60. Ramos VF, Pinheiro OS, Ferreira da Costa E, Souza da Costa AO. A method for exergetic analysis of a real kraft biomass boiler. Energy. 2019;183:946-57.
61. Fathian Sabet A, Bararzadeh Ledari M, Maleki F, Fani M. Exergy and thermoeconomic comparison of sustainable methanol and ammonia production from waste and CO_2. Journal of Environmental Chemical Engineering. 2025;13(5).
62. Qingchun Y, Zhi Z, Yingjie F, Genyun C, Dawei Z, Jianhua Y. Advanced exergy analysis and optimization of a CO2 to methanol process based on rigorous modeling and simulation. Fuel. 2022;325:124944.
63. Achomo MA, Muthukumar P, Peela NR. Thermodynamic, energy and exergy analysis of steam reforming of methanol for hydrogen production. Int J Hydrogen Energ. 2025;149.
64. Jan S. Chemical exergies of the elements. Appl Energ. 1989;32(4):269-86.
65. Szargut J. Exergy method: Technical and ecological applications: WIT Press; 2005.
66. Parvez AM, Wu T, Li S, Miles N, Mujtaba IM. Bio-DME production based on conventional and CO2-enhanced gasification of biomass: A comparative study on exergy and environmental impacts. Biomass and Bioenergy. 2018;110:105-13.
67. Bongartz D, Burre J, Mitsos A. Production of Oxymethylene Dimethyl Ethers from Hydrogen and Carbon Dioxide—Part I: Modeling and Analysis for OME1. Ind Eng Chem Res. 2019;58(12):4881-9.

Reaction Chemistry & Engineering Accepted Manuscript

68. Max S. Peters, Timmerhaus KD, West RE. Plant Design and Economics for Chemical Engineers. 5. ed: McGraw-Hill; 2002.
69. Turton R, Shaeiwitz JA, Debangsu B, Whiting WB. Analysis, Synthesis, and Design of Chemical Processes. 5 ed: Pearson Education; 2018 June 22, 2018.
70. Jenkins S. 2024 CEPCI updates: June (prelim.) and May (final): Chemical Engineering magazine; 2024 [updated August 16, 2024. Available from: https://www.chemengonline.com/2024-cepci-updates-june-prelim-and-may-final/.
71. Bank EC. Average Annual Exchange EUR vs. USD [
72. Friedemann GA, Daniel HK, Nadine B, Ralph-Uwe D. A standardized methodology for the techno-economic evaluation of alternative fuels – A case study. Fuel. 2017;194:511-26.
73. Bortolotti AAaM. Clean Hydrogen Monitor. 2022.
74. Antzaras AN, Papalas T, Heracleous E, Kouris C. Techno–economic and environmental assessment of CO2 capture technologies in the cement industry. Journal of Cleaner Production. 2023;428.
75. Bundesnetzagentur. Energiemarkt aktuell - Entwicklung der Industriestrompreise: Bundesnetzagentur - SMARD; 2025 [updated 11.02.2025. Industrial electricity price]. Available from: https://www.smard.de/page/home/topic-article/444/215830/entwicklung-der-industriestrompreise.
76. Tan EC, Talmadge M, Dutta A, Hensley J, Snowden-Swan LJ, Humbird D, et al. Conceptual process design and economics for the production of high-octane gasoline blendstock via indirect liquefaction of biomass through methanol/dimethyl ether intermediates. Biofuels, Bioproducts and Biorefining. 2016;10(1):17-35.
77. Bustillo-Lecompte CF, Mehrvar M, Quinones-Bolanos E. Cost-effectiveness analysis of TOC removal from slaughterhouse wastewater using combined anaerobic-aerobic and UV/H2O2 processes. J Environ Manage. 2014;134:145-52.
78. James G, Witten D, Hastie T, Tibshirani R. An Introduction to Statistical Learning. 2 ed: Springer New York; 2021.
79. D'Ambrosio A, Facchino M, Tatarelli S, Piemonte V, Capocelli M, De Falco M. Carbon capture utilization through a novel multistage configuration for dimethyl ether synthesis. Journal of Cleaner Production. 2025;490.
80. D'Ambrosio A, de Oliveira Campos BL, Sauer J, Piemonte V. Multi-stage direct synthesis of dimethyl ether: Integrated thermodynamic, economic and environmental assessment for process intensification. Chem Eng J. 2026;542.

Reaction Chemistry & Engineering Accepted Manuscript

Data will be made available upon request.

Reaction Chemistry & Engineering Accepted Manuscript